A Study of the Mobility of Silver Ions in Chitosan Membranes

by

Elaine Yi-Hua Lin

A thesis
presented to the University of Waterloo
in fulfillment of the
thesis requirement for the degree of
Master of Applied Science
in
Chemical Engineering

Waterloo, Ontario, Canada, 2007

AUTHOR'S DECLARATION

I hereby declare that I am the sole author of this thesis. This is a true copy of the thesis, including any required final revisions, as accepted by my examiners.

I understand that my thesis may be made electronically available to the public.

Abstract

Chitosan membrane has found applications in biomedical, wastewater treatment, and petrochemical fields that involve the use of silver ions (Ag^+). However, mobility of Ag^+ in chitosan membranes has seldom been studied. In this study, transport properties of Ag^+ in chitosan membranes are studied in-depth, to determine diffusivity coefficient, permeability coefficient, and sorption uptake of Ag^+ in chitosan. All parameters are evaluated based on the influence of feed concentration, membrane thickness and operating temperature.

The diffusivity is determined from the time lag obtained from transient diffusion experiments. The permeability is determined from the steady state of permeation experimentally. The diffusivity and corresponding permeability coefficients of Ag^+ in chitosan range from 6.8×10^{-9} to 2.0×10^{-7} (cm^2/s) and from 6.6×10^{-8} to 2.0×10^{-7} {mol m/[m^2 s (mol/L)]}, respectively, over the conditions tested. Temperature dependencies of these two parameters are found to follow the Arrhenius relationship.

Sorption uptake of the silver salt in chitosan correlates well with the Langmuir isotherm. Also determined from the sorption tests are degree of membrane swelling at different concentrations. This information allows diffusivity coefficients to be determined from the steady state permeation rate. These values of diffusivity are compared with that obtained using the time lag method.

Acknowledgements

I would like to take this opportunity to thank those who have guided, supported, and accompanied me throughout my master's study at the University of Waterloo.

My greatest gratitude goes to my supervisor, Dr. Xianshe Feng, for his invaluable guidance and constructive advice throughout the course of this study and in preparation of a paper and this thesis. I would also like to thank Dr. Mark Pritzker and Dr. Ali Elkamel for their careful review of my thesis as well as Jennifer Du, Eddie Xiao, and Dr. Li Liu for their recommendations and help with my experiments.

I am very thankful to my parents who were always proud of me and supported me unconditionally. Their care and encouragement were one of the most essential elements of my strength in completing this master's degree. I am also grateful for my housemates and friends Ingrid Yao, Christina Wei, and Flora Chui who stood by my side and encouraged me at times of hardship as well as shared with me much laughter throughout the two years. Furthermore, I would like to thank my brothers and sisters at KWCAC and TLCF for their prayers and support.

Last but not least, I am especially grateful for my Heavenly Father for His incredible love, support, and guidance in my life.

Financial support from the Natural Sciences and Engineering Research Council (NSERC) of Canada in the form of research grant and postgraduate scholarship is gratefully acknowledged.

To my parents Fu-Yuan Lin and Li-Fang Chen, and my brother Joey Lin

Table of Contents

List of Figures

List of Tables

Chapter 1

Introduction

1.1 Background

Chitosan is a biopolymer derived by deacetylation of chitin, an abundant biopolymer obtained mainly from shellfish waste as a byproduct of the seafood industry. Due to the amino ($-NH_2$) and hydroxyl ($-OH^-$) groups in its structure that function as ligands, chitosan is a chelating polymer with excellent adsorption capacities for a number of metal ions. Chitosan is also characterized by being cationic, biocompatible, and antibacterial. These characteristics allow chitosan to find wide applications as a material in biomedical processes, food industry, and water purification. It has been documented that, in the past decade, there are three areas of potential applications for chitosan that involve incorporating or adsorbing silver ions (Ag^+) into chitosan membranes:

- as a potential base membrane to accommodate a silver facilitating agent for olefin/paraffin separation [1]
- as a biomaterial for controlled release of silver compounds for wound dressing [2,3]
- as an adsorbent for recovering silver from industrial wastewater [4-7]

Despite these applications involving Ag^+ in chitosan membranes where information regarding mobility of Ag^+ is significant, the transport properties of Ag^+ or even other metal ions in chitosan have seldom been mentioned in the literature.

It is the goal of the present work to study the mobility of Ag^+ in chitosan by evaluating the transport properties of Ag^+ in chitosan membranes. The scope of the work includes experimentally determining the permeation properties, permeability coefficients and diffusivity coefficients of Ag^+ in chitosan. The diffusivity coefficient is determined from the transient response of permeation experiments using the time lag method and the permeance and permeability coefficients from the steady state of permeation. In addition, the sorption uptake of Ag^+ in chitosan membranes at equilibrium is also determined. In evaluating these properties, the effects of three experimental variables were investigated: feed concentration, membrane thickness and operating temperature.

To our knowledge, this is the first time the transport properties of Ag^+ within chitosan membranes were studied in depth. This study is expected to provide information that is fundamental to the various applications involving Ag^+ with chitosan membranes.

1.2 Outline of the Thesis

This thesis includes the following sections: Chapter 1 gives a brief background, research initiatives, scope and objectives of this study. A detailed background review of the literature on the related subjects is presented in Chapter 2. This chapter also includes the theoretical background of diffusion and adsorption, which is used to analyze the experimental data in this study. Chapter 3 outlines the method of membrane preparation and

procedures for the two parts of the experimental work – permeation and sorption tests. In Chapter 4, the results from both permeation and sorption tests investigating the effect of feed concentration, membrane thickness, and operating temperature are summarized and analyzed. A comparison between the diffusivity coefficients obtained using the steady state permeation rate and time lag is also presented in this chapter. Finally, the conclusions drawn from this study and recommendations for future work are given in Chapter 5.

Chapter 2

Literature Review

2.1 Chitosan

2.1.1 Source, Structure and Manufacturing

Chitosan is a polymer derived from chitin, the second most abundant natural polymer and naturally occurring polysaccharide found in shells of crustaceans, cell walls of fungi and exoskeletons of insects [8-10].

Chemically, chitin is known to be a long polymer chain of β(1→4) linked 2-acetamido-2-deoxy-β-D-glucose units [11] and chitosan is its N-deacetylated product [12]. Both can be considered to be analogues of cellulose, where the hydroxyl groups at carbon-2 have been replaced by the acetamido and amino groups, respectively [11,13] (Fig. 2.1). Chitosan was first discovered in 1859 by boiling chitin in concentrated potassium hydroxide (KOH) [14]. It was then formally named chitosan by Hoppe-Seyler in 1894 [14,15].

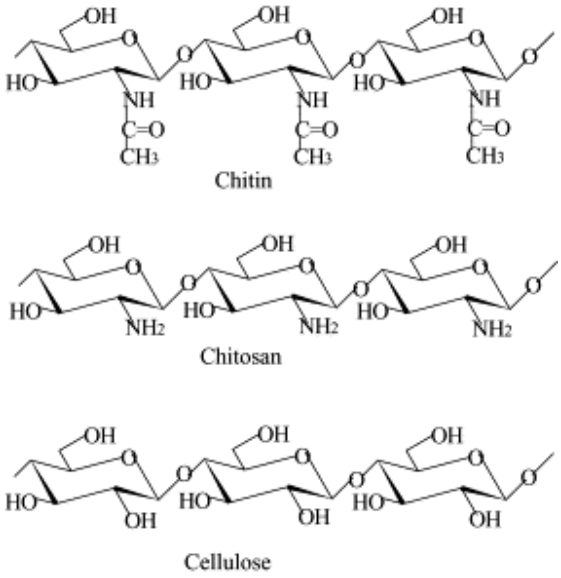

Figure 2.1 Structure of chitin, chitosan, and cellulose

Commercially, chitin and chitosan are obtained from shellfish wastes of the seafood processing industry (mainly shells of crabs, krills and shrimps) [4,12,16-18]. The process of using shell materials to produce chitin and then chitosan is illustrated in Fig. 2.2. It involves removal of proteins from the shell material by sodium hydroxide (NaOH) solution, followed by extraction of minerals such as calcium carbonate and calcium phosphate using hydrochloric acid (HCl). The resulting material, chitin, is then treated with 40-45% NaOH solution to hydrolyze the N-acetyl linkage (i.e., deacetylation), followed by purification procedures to produce chitosan [11,18,19]. At this stage, the product can be dried to give flaked chitosan [18]. It should be noted that chitosan in its free amine form is not soluble in water. At acidic pH's (pH<6.5), the free amino groups ($-NH_2$) are protonated to become cationic amine groups ($-NH_3^+$), thereby forming chitosanium salts. Therefore, acid is generally required to prepare aqueous solutions of chitosan [11,18].

Chitosan is a versatile biomaterial available in many useful forms that can be readily obtained or are commercially available. Some forms being pursued commercially are: film, fiber, beads, gels, paste, solutions and microcrystalline powders [18,20].

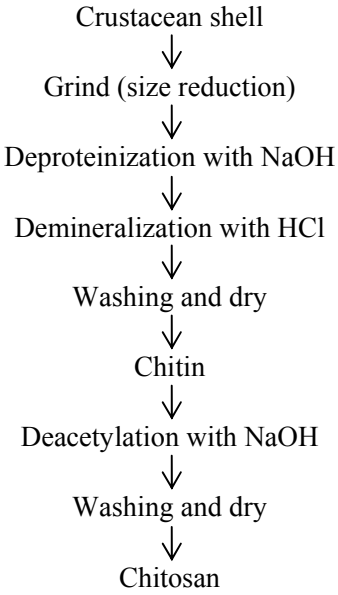

Figure 2.2 Manufacturing process of chitin and chitosan

2.1.2 Properties and Applications

Chelating Property – Wastewater Treatment

One of the most important properties of chitosan is the ability to chelate heavy metal ions [15]. With the nitrogen electrons, the amino groups on chitosan serve as ligands or binding sites for metal ions, forming metal complexes. Chitosan is capable of chelating many metal ions including iron, copper, magnesium, silver, cadmium, mercury, lead, nickel,

zinc, manganese, chromium and uranium [9,15,21]. As a result, chitosan is a promising adsorbent to remove heavy metal ions from industrial wastewater.

Cationic Property – water purification, food industry, cosmetics

The amino group also makes chitosan a cationic polyelectrolyte. When dissolved in acidic media at pH<6.5, chitosan possesses a high positive charge density, allowing it to interact with negatively charged surfaces. This property makes chitosan an excellent flocculent to aggregate with negatively charged colloids [11,18]. Being a flocculent and having the ability to chelate iron, chitosan is a useful pool and spa clarifier [18]. In the food industry, chitosan has been used for coagulation of suspended solids from food processing waste [21,22]. In addition, its ability to bind to negatively charged fats and lipids and its film forming capacities make chitosan a potential candidate for food packaging applications [23]. Due to its adherence to skin and hair that are composed of negatively charged proteins and mucopolysaccharides, chitosan is also useful in cosmetics or personal care products [18].

Biological Properties – medicine, biotechnology and agriculture

Chitosan is a natural polymer that is biocompatible, non-toxic, biodegradable and physiological inert [11,18]. These biological characteristics provide chitosan a wide spectrum of applications. In the medical field, for example, chitosan is a candidate for wound healing treatment [2,18,22,24,25] due to its water-absorption, biocompatibility and oxygen permeability. It may also be used in drug delivery [22,26] and drug controlled release systems [27]. With its excellent film forming capabilities, it has a potential application as contact lenses [25,28]. In biotechnology, chitosan has been used as enzyme

and cell immobilization supports [11,22]. In agriculture, chitosan can be used as seed coating or soil additive to increase crop yields [18,29]. Very importantly, since chitosan is a biodegradable polymer, it is eco-friendly and safe for humans and the environment [11].

In addition to the above applications, chitosan is also used for paper making, textile finishing and in photographic processes [21]. Furthermore, because of its excellent hydrophilicity, chitosan has also shown to be a suitable membrane material for solvent dehydration by pervaporation [30,31].

2.2 Applications of Chitosan with Silver Ions

In the past decade, chitosan membrane has found potential applications that involve incorporation of silver ions (Ag^+). These applications include facilitated transport using Ag^+-incorporated chitosan membranes, chitosan wound dressing incorporating silver compounds, and silver recovery from wastewater using chitosan as an adsorbent.

2.2.1 Facilitated Transport – Olefin/Paraffin Separation

Carrier-facilitated transport membranes incorporate a reactive carrier that helps transport one of the components of the feed across the membrane. In the process, the feed mixture is contacted with the membrane on the upstream side. The carrier selectively and reversibly complexes the component of interest and diffuses to the downstream membrane interface where the reaction is reversed and the component is recovered.

The dominant technology for olefin/paraffin separations in the petrochemical industry is low-temperature and high-pressure distillation that is highly energy-intensive due to

similar volatilities between an olefin and its associated paraffin. Work has been done since the 1980s to employ facilitated transport as a possible alternative to the conventional distillation process [32]. Since silver reacts with olefins specifically and reversibly by forming an olefin-silver complex, it has been a popular choice as an olefin carrier for facilitated transport [33-38]. The olefins are able to form a reversible complex with Ag^+ and thus pass through the membrane through the physical solution-diffusion mechanism as well as the chemically facilitated transport, while paraffins permeate through the membrane via solution-diffusion only. It was documented that the separation performance of silver-based polymer electrolyte membranes was remarkably high [34,36]. Furthermore, recent studies in our lab showed that chitosan serving as a base membrane to incorporate a silver facilitating agent was one of the most effective for olefin/paraffin separation as compared to other base membranes [1].

2.2.2 Wound Dressing

Ag^+ is known to possess excellent antibacterial properties [5,24,39]. For burn injuries where the normal skin barrier and host defense mechanisms that prevent infection are disrupted, the use of silver compounds such as silver sulfadiazine (AgSD) is believed to be an effective treatment to prevent infection as they offer high antibacterial activity [40]. As a novel biomaterial well known for accelerating healing of wounds, chitosan is suited for the manufacture of wound dressings [41,42]. In recent years, chitosan membranes have been shown to be a potential wound dressing to incorporate AgSD for treatment of burn injuries [2,3]. AgSD-incorporated chitosan membrane serves as a rate-controlling reservoir to release silver compounds to the wounds in a sustained way. This provides an alternative to the

traditional method of direct application of AgSD cream that has raised concerns with potential silver toxicity. In addition, this material gives more effective long-term inhibition of bacterial growth, reducing the frequency of cream application that causes discomfort for patients and require substantial nursing effort.

2.2.3 Silver Recovery from Wastewater

In the past decade, concerns have been raised about the presence of soluble silver in wastewater from industrial processes (including photographic and electroplating industries) due to its toxicity to aquatic organisms [4,5]. Being a valuable metal, silver has been recovered by several methods [4]. Chitosan has been known for its ability to adsorb metals and has been described as an excellent metal adsorbent since 1970s. It has also been documented as an effective means to remove silver from aqueous solutions [4-7].

Compared to existing recovery methods such as precipitation and ion-exchange, the use of chitosan as a base material for silver recovery has many advantages including lower operating cost, the avoidance of formation of a sludge that is expensive to refine [4] and effectiveness even at low ionic concentrations [15]. Although efficient removal of certain anionic silver salts present in industrial effluents is yet to be developed, the binding behavior of chitosan to Ag^+ was found to be largely comparable to that of commercial resins. High selectivity, high adsorption capacity, and easy recovery of silver from chitosan resin were also documented [5]. Based on the information in the literature, chitosan appears to be an attractive candidate for recovery of Ag^+ from industrial wastewater.

2.3 Studies Regarding Ag^+ Mobility in Chitosan

All applications mentioned in the previous section involve transport of Ag^+ in chitosan. However, the transport properties of Ag^+ (or even other metal ions) in chitosan have seldom been reported in the literature. One exception is the study by Karajewska [13], who investigated the diffusion of 15 metal ions, including Ag^+. Only the permeability coefficients of the ions were determined, and the focus lay on the comparison between the metal ions and neutral non-electrolytes in terms of two transport models. Another study concerning transport of metal ions in chitosan was that by Du et al. [43], who determined the permeation rate of six metal ions in silk a fibroin/chitosan blend. However, Ag^+ was not studied and the aim was to determine the effect of the composition of chitosan blend membranes on the permeation rate and permeability coefficient of K^+. There is little work reported in the literature that deals with the mobility of Ag^+ in chitosan in depth to provide fundamental and useful information for practical applications.

2.4 Transport through Membranes

2.4.1 Solution-Diffusion Mechanism

As chitosan membrane is non-porous, the transport of a silver salt compound follows the solution-diffusion mechanism, whereby the solute dissolves into the membrane and diffuses across through the free volume of the membrane. The most widely adopted model to describe solute transport through a membrane is schematically shown in Fig. 2.3 [44].

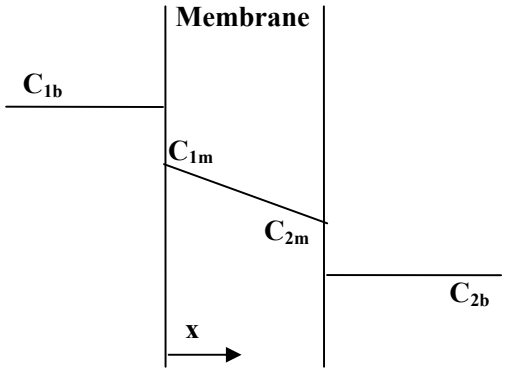

Figure 2.3 Concentration profile for solute transport across the membrane

The solute is transported from the feed side (higher concentration) to the downstream side (lower concentration) via the following series of steps:

1. diffusion from the bulk solution to the membrane surface
2. sorption into the membrane
3. diffusion across the membrane
4. desorption at the downstream side of the membrane
5. diffusion to the bulk solution in the permeate

Each step represents a resistance, but step 3 in general is rate determining step. The effects of the boundary layers (steps 1 and 5) are often assumed to be negligible. This assumption is most valid when the concentration gradient across the membrane is large, the solution on both sides of the membrane is well stirred or the overall resistance is dominated by the membrane. All these criteria are satisfied in this study due to the nature of chitosan and the experimental set-up, as discussed later.

2.4.2 Fick's Law of Diffusion

When no chemical interactions between the solute and the membrane take place, the transport of components inside a non-porous membrane is described by molecular diffusion, which may be described by Fick's first law:

$$J = -D\frac{\partial C_m}{\partial x} \qquad (2.1)$$

where J is the rate of transfer per unit area of section, called the permeation rate or diffusion flux, C_m is the concentration of diffusion substance in the membrane, x is the length measured normal to the membrane section, and D is the diffusivity coefficient. If diffusion occurs effectively in one direction only and the diffusivity coefficient is constant with respect to concentration and does not vary from point to point, Fick's second law of diffusion gives:

$$\frac{\partial C}{\partial t} = D\frac{\partial^2 C_m}{\partial x^2} \qquad (2.2)$$

Consider the diffusion through a plane membrane of thickness l where constant concentrations, C_{1m} and C_{2m}, are maintained at the membrane surfaces x = 0 and x = l, respectively. At the steady state, the permeation rate can be derived from Eq. 2.1 as

$$J = \frac{D(C_{1m} - C_{2m})}{l} \tag{2.3}$$

In some cases where the concentrations of the diffusing substance on each side of the membrane surface are not readily known, the permeation rate can be written as:

$$J = \frac{P(C_{1b} - C_{2b})}{l} = P'(C_{1b} - C_{2b}) \tag{2.4}$$

where C_{1b} and C_{2b} are the bulk concentrations on the upstream and downstream sides of the membrane, respectively. Eq. 2.4 defines the permeability coefficient (P) and the permeance (P'). If a linear relationship exists between the bulk concentration and the concentration of the diffusing substance at the membrane surface, the sorption isotherm will be linear and can be described by Eq. 2.5 where S is the solubility of the diffusing substance in the membrane.

$$C_m = SC_b \tag{2.5}$$

From Eqs. 2.3-2.5, one can find that the permeability coefficient (P) is a function of both diffusivity coefficient (D) and solubility (S), as shown in Eq. 2.6.

$$P = DS \tag{2.6}$$

In terms of its physical meaning, the diffusivity coefficient is related to the ability of diffusing substances to move in the polymeric network and can be considered as a measure of the rate at which the individual molecules move within the membrane. The permeability coefficient can be considered as the total count of diffusing substances moving across the membrane from a point of view outside of the membrane. In other words, the permeability coefficient is related to the global measurement of the rate of transport across the membrane, given in terms of the measurable changes in the concentrations in the bulk solutions on both sides of the membrane, while the diffusivity coefficient characterizes the mobility within the membrane, described quantitatively in terms of the concentration within it [45,46].

Solubility is a measure of sorption uptake, which measures the maximum capacity of the sorbate in the membrane at specific conditions (adsorbent concentration, temperature, etc.)

2.4.3 Time Lag Method for Determination of Diffusivity

The time lag method to study permeation was originally conceived by Daynes [47] followed by Barrer [48]. It allows diffusivity to be directly evaluated from experimental data without needing intensive mathematical treatment as required by other techniques [49]. Consider a diffusion process across the membrane down a concentration gradient and that the following conditions apply: the diffusivity coefficient is constant, the membrane is originally free of diffusing substances, and the concentration of the diffusing substance on the downstream side is negligibly low ($C_{2b} = 0$). Suppose at $t = 0$, the feed at a constant concentration C_{1b} is in contact with the membrane. Thus, by integrating Eq. 2.2 with respect to time, the amount of diffusant Q_t that has passed through the membrane over the duration t can be expressed by Eq. 2.7[50]:

$$\frac{Q_t}{lC_{1m}} = \frac{Dt}{l^2} - \frac{1}{6} - \frac{2}{\pi^2}\sum_{1}^{\infty}\frac{(-1)^n}{n^2}\exp\left(\frac{-Dn^2\pi^2 t}{l^2}\right) \tag{2.7}$$

As time approaches infinity, the permeation rate approaches a steady level, and Q_t becomes

$$\frac{Q_t}{lC_{1m}} = \frac{Dt}{l^2} - \frac{1}{6} \tag{2.8}$$

The graph of Q_t vs. t yields a straight line represented by

$$Q_t = \frac{DC_{1m}}{l}\left(t - \frac{l^2}{6D}\right) \tag{2.9}$$

which upon extrapolating to the t-axis will yield an intercept τ, where

$$\tau = \frac{l^2}{6D} \tag{2.10}$$

τ is the so-called "time lag" of diffusion, and is associated with the time necessary for the permeation rate to reach steady state. With Eq. 2.10, the diffusivity coefficient (D) can be determined directly from permeation measurements over the transient period of diffusion. From the steady state of the permeation, permeability can be deduced using Eq. 2.4 [50,51]. As will be shown later, the diffusivity coefficient of Ag^+ in chitosan is in fact affected by concentration. As a result, the diffusivity determined by the time lag method is the overall "apparent diffusivity".

Although the time lag method is the most common method used to determine gas diffusion coefficients in polymer membranes [52,53] and its use for gas diffusion and related work is common [49,52-57], it has rarely been used for ionic diffusion. Among the very few documented studies that use time lag for ionic diffusivity in polymer membranes, there were discrepancies in the results [44] and sometimes the transport process was not really diffusion under a concentration gradient as the driving force [58]. As far as we know, the work presented here is the first case where the time lag method is applied directly to ionic diffusivity in diffusion, where the experimental results showed a considerable degree of consistency.

2.4.4 Temperature Dependency of Permeation Properties

The Arrhenius equation is often utilized for correlation of permeation properties in gas permeation [57,59]. Permeability and diffusivity coefficients are expressed as the following when the Arrhenius relationships are followed:

$$P = P_0 \exp\left(\frac{-E_p}{RT}\right) \tag{2.11}$$

$$D = D_0 \exp\left(\frac{-E_d}{RT}\right) \tag{2.12}$$

where E_p and E_d are the energies of activation for permeation and diffusion (kJ/mol), respectively, P_0 [mol m/m^2 s (mol/L)] and D_0 (cm^2/s) are the respective pre-exponential factors, R is the gas constant (J mol/K), and T is the temperature (K). Eqs. 2.11 and 2.12 can be linearized by taking natural logarithms to yield:

$$\ln P = -\frac{E_p}{RT} + \ln P_0 \tag{2.13}$$

$$\ln D = -\frac{E_D}{RT} + \ln D_0 \tag{2.14}$$

Therefore, if the Arrhenius relationships are followed, plots of ln P and ln D versus $\frac{1}{T}$ will give straight lines with slopes of $-\frac{E_p}{R}$ and $-\frac{E_D}{R}$ and intercepts of ln P_0 and ln D_0, respectively. In addition, the temperature dependency of solubility can normally be expressed by:

$$S = S_0 \exp\left(\frac{-\Delta H_s}{RT}\right) \tag{2.15}$$

where ΔH_s is the heat of sorption (kJ/mol). From Eqs. 2.6 and 2.13-2.15, it can be seen tat ΔH_s is related to the activation energy by:

$$\Delta H_s = E_p - E_d \tag{2.16}$$

A positive ΔH_s indicates that the sorption of the permeant in the membrane is endothermic and that the sorption uptake will increase with an increase in temperature. A negative ΔH_s indicates exothermic sorption and that the sorption capability will decrease with temperature.

2.5 Equilibrium Models of Adsorption

The adsorption isotherms provide information on the maximum uptake of adsorbates at a given feed concentration and relate the coverage of the adsorbates on the adsorbent with the concentrations of the adsorbate in the solution. The Langmuir and Freundlich models are among the most commonly used to describe equilibrium sorption isotherms.

2.5.1 The Langmuir Equation

Langmuir was the first to propose a theory of adsorption onto a flat surface from a kinetic viewpoint. The Langmuir theory is based on the principle that the rate of adsorption onto the surface and the desorption rate from the surface are equal when an adsorption equilibrium is reached [60]. Assumptions of the Langmuir model include:

- Homogeneous adsorbent surface (i.e. adsorption energy is constant at all adsorption sites),
- Localized adsorption on surface (i.e. adsorbed atoms or molecules are adsorbed at definite, localized sites), and
- Each adsorption site can accommodate only one molecule or atom.

The Langmuir equation, valid for monolayer sorption onto a homogeneous surface with definite, localized sites, is given by:

$$\theta = \frac{bC_e}{1 + bC_e} \tag{2.17}$$

where θ is the fractional coverage (dimensionless), C_e is the adsorbate concentration in the liquid phase at equilibrium (mg/L), and b is the affinity constant or Langmuir constant, a measure of the affinity of an adsorbate molecule for the surface. For a larger b, the coverage of the adsorbent surface by adsorbate molecules is greater at a given adsorbate concentration in the liquid phase due to the stronger affinity of adsorbate molecules towards the adsorption sites. The fractional coverage θ can be described as the ratio of q_e, the amount of adsorbate adsorbed by the adsorbent at equilibrium (mg/g) to q_{max}, the maximum amount that can be adsorbed (mg/g):

$$\theta = \frac{q_e}{q_{\max}} \tag{2.18}$$

The Langmuir model can be rearranged to yield:

$$\frac{C_e}{q_e} = \frac{1}{q_{\max}} C_e + \frac{1}{q_{\max} b} \tag{2.19}$$

Consequently, a plot of $\frac{C_e}{q_e}$ vs. C_e will result in a straight line of slope $\frac{1}{q_{\max}}$ and intercept $\frac{1}{q_{\max} b}$. This linear relationship can be used to determine the validity of the Langmuir model, and to determine the maximum adsorption amount q_{max} and the Langmuir constant b from experimental equilibrium sorption data [61].

2.5.2 The Freundlich Equation

In some adsorption processes, fundamental adsorption isotherm equations such as the Langmuir equation are not adequate because the basic assumptions in the Langmuir model

are not readily satisfied. For example, a heterogeneous surface and multi-site adsorption may be encountered [61]. To this end, empirical approaches have been proposed to describe the equilibrium data. One of the earliest empirical models used was the Freundlich equation [60] given by:

$$q_e = kC_e^n \tag{2.20}$$

where k [(mg/g)/(L/mg)^n] and n (dimensionless) are Freundlich constants indicating sorption capacity and intensity, respectively [62]. The linearized form of Eq. 2.19 is:

$$\log q_e = \log k + n \log C_e \tag{2.21}$$

If the Freundlich model applies to the equilibrium sorption data, a logarithmic plot of q_e vs. C_e will yield a straight line with a slope of n and an intercept of $\log k$.

In the literature, both the Langmuir and Freundlich models have been used to fit experimental equilibrium sorption data. Table 2.1 summarizes the models used for several systems involving chitosan. Despite the fact that metal sorption on chitosan takes place inside the material rather than merely on the external surface, some have found that the sorption of metals fits the Langmuir equation. Others, on the other hand, have found that sorption follows Freundlich behavior. The discrepancy is mainly caused by the differences in the types of chitosan used and the experimental conditions.

Table 2.1 Isotherm models for equilibrium sorption data of different metals on chitosan in the literature

Adsorbate	Concentration (mg/L)	Adsorbent	Adsorption Models	Reference
Cd(II)[a]	0 – ~60	Crushed crab shell chitosan	Freundlich	[6]
$FeSO_4$, $FeCl_3$	2 – 14	Chitosan beads	Langmuir	[62]
$CuSO_4$	62.7 – 75.3	Chitosan particles	Langmuir	[63]
$Pb(NO_3)_2$	10 – 1000	Chitosan particles	Freundlich	[64]
$K_2Cr_2O_7$	500	Chitosan coated oil palm shell charcoal	Langmuir	[65]
$Cr_2(SO_4)_3$	0.015-1.73	Chitosan granules	Langmuir	[66]
$NiSO_4$	~20 – 400	Chitosan resins	Freundlich	[67]

[a] The anions are not disclosed.

Chapter 3

Experimental

In this study, the transport parameters determined experimentally include permeability coefficient and diffusivity coefficient of Ag^+ in chitosan, as well as sorption uptake of $AgNO_3$ in chitosan. The first two parameters are determined from the permeation tests, and the third in the sorption tests. Table 3.1 lists the three variables and their range evaluated in both tests. The net membrane thickness is referred to the thickness of the dry chitosan membrane before being used in the permeation and sorption tests.

Diffusivity has a dimension of length square over time, and the unit used in this study is (cm^2/s). Permeability is sometimes also given a unit of (cm^2/s) in the literature [13,43,44]. Due to the different physical meaning between the two parameters, the unit of {mol m/[m^2 s (mol/L)]} is used for permeability in this study to characterize the permeation rate normalized by the concentration gradient (i.e. the driving force). Sorption uptake is represented in mass ratio as (g silver nitrate/g chitosan).

Table 3.1 Range of evaluation for each of the three variables in permeation and sorption tests

	Feed concentration (M)	Net membrane thickness (μm)	Temperature (ºC)
Permeation test	0.08 – 1	20 – 50	21 – 61
Sorption test	0 – 1	16 – 51	23 – 63

3.1 Materials

Membranes used in this study were prepared from chitosan flakes (Flonac N, molecular weight 100,000) supplied by Kyowa Technos Co. Ltd., Japan. Silver nitrate ($AgNO_3$), acetic acid, and sodium hydroxide were purchased from Aldrich Chemical Company. De-ionized laboratory water was used in the aqueous solutions for membrane preparation and treatment.

$AgNO_3$ was chosen as the silver compound for this study due to its lower cost compared to other silver compounds such as silver tetrafluoroborate ($AgBF_4$), silver perchlorate ($AgClO_4$) and silver triflate ($AgCF_3SO_3$). It should be noted that in the permeation experiment, it is the coupled Ag^+ and NO_3^- ions that are moving, rather than merely Ag^+ ions by itself because electro-neutrality is always maintained.

3.2 Membrane Preparation

Homogeneous dense chitosan membranes were prepared by the solution casting technique. Chitosan flakes were dissolved in dilute acetic acid solution by the protonation of the amine groups of chitosan to form a homogeneous solution. The polymer solution, comprising 1.1 wt.% chitosan, 2 wt.% acetic acid and 96.9 wt.% water, was filtered and then cast onto a horizontally positioned glass plate with a casting knife. By adjustment of the size of the casting gap, the amount of solution and consequently the resulting thickness of the product membrane were controlled. The cast chitosan solution film was air-dried in an environmentally controlled chamber supplied by D.F.S. Inc., France. The dried membrane in

the form of a chitosan salt was then subjected to alkaline treatment by 1M sodium hydroxide solution for 24h, to convert the cationic amine groups ($-NH_3^+$) into the free amine form ($-NH_2$). The resulting membrane was rinsed thoroughly by de-ionized water, cut into membrane samples of same cross-sectional areas, and dried in vacuum. The original thicknesses of the dried membrane samples were measured using a digital micrometer supplied by Mitutoyo Inc. The original membrane thicknesses of the membranes so formed were between 15 and 36μm. Thicker membranes were prepared by a similar method except that the chitosan polymer solution was poured into Petri dishes instead of cast on glass plates. Finally, membrane samples were stored in de-ionized water for permeation tests or stored under room temperature for sorption tests.

3.3 Permeation Tests

The apparatus used in the permeation tests is shown schematically in Fig. 3.1. The vertical permeation cell consists of two compartments, a feed compartment of 125mL and a receptor compartment of 2L. A piece of wet chitosan membrane (that had been stored in de-ionized water prior to the test) with a cross-sectional area of 10.8 cm^2 separated the two compartments and was mounted horizontally against the opening of the feed compartment and sealed by a plastic ring to ensure that the solution within the feed compartment did not leak to the receptor compartment. Before the measurement started, the receptor compartment was filled with 1.5 L of de-ionized water.

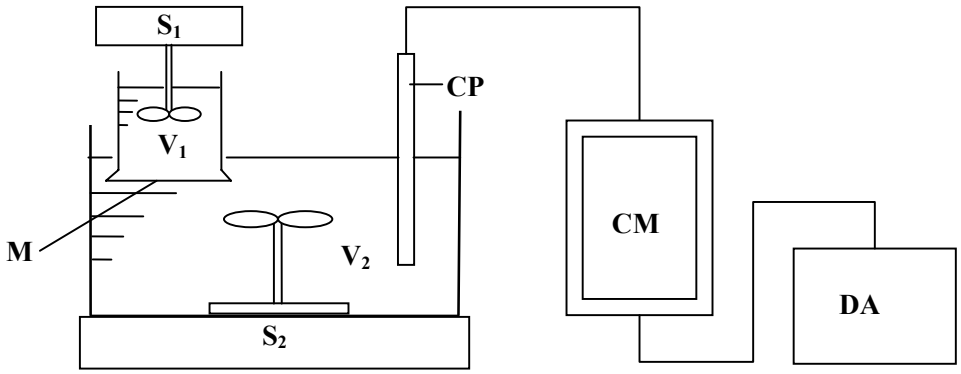

Figure 3.1 Schematic view for permeation test set-up. V_1, V_2, feed and receptor compartment, respectively. M, membrane. S_1, S_2, mechanical and magnetic stirrer for V_1 and V_2, respectively. CP, conductivity measuring probe. CM, conductivity meter. DA, data acquisition system.

At the beginning of the measurement (time zero), 50mL of $AgNO_3$ solution of known concentration was charged into the feed compartment. Throughout the test, the liquids in both compartments were stirred continuously, by a magnetic stirrer in the receptor compartment and by a mechanical stirrer in the feed compartment. As a result of the diffusion process of $AgNO_3$ from the high-concentration feed solution to the low-concentration receptor solution, the concentration of $AgNO_3$ in the receptor compartment gradually increased from zero from the start of the measurement. The change in the concentration of $AgNO_3$, an ionic compound, in the receptor compartment was determined by recording the conductivity of the solution. This was performed by a conductivity probe, which was immersed in the receptor solution and was connected to an inoLab Cond Level 2 conductivity meter that provided the conductivity readings. Data from the conductivity meter was transmitted to MultiLab pilot data acquisition software that stored the conductivity

data as a function of time. For the permeation test, the conductivity data were logged at five-second intervals from time zero to a time after the steady state of permeation was reached. The measured conductivity was correlated to $AgNO_3$ concentration by previously established concentration-conductivity calibration curves. Therefore, the measurement of conductivity in the receptor compartment over time could be related to the permeation rate of $AgNO_3$ across the chitosan membrane.

All permeation tests, except for those where the effect of temperature was evaluated, were carried out at room temperature. For experiments at higher temperatures, the solutions in both compartments were pre-heated to the desired temperature and a heating plate equipped with a build-in magnetic stirrer was placed under the permeation cell throughout the test to maintain the desired temperature.

It should be pointed out that during the course of each permeation experiment, the $AgNO_3$ concentration in the feed compartment was much higher than that in the receptor compartment so that the variation in the feed $AgNO_3$ concentration was negligibly small. This satisfies one of the conditions used to derive the time lag equation.

3.4 Sorption Tests

Prior to the sorption process, chitosan membranes of equal cross-sectional areas (12.2 cm^2) are dried in vacuum. The original weights (m_o) and original thicknesses (l_o) of the dried membranes were measured. Chitosan membranes were then immersed in 40mL of $AgNO_3$ solutions of known concentration over a period of at least 24h. Upon removal, the

membranes' surface water was quickly blotted and the wet weights (m_w), i.e., weight of the chitosan membrane sorbed with both water and $AgNO_3$, were measured. The wet thicknesses (l_w) of the membranes were measured using the micrometer right after measurement of the wet weights. The membrane samples were then dried in vacuum at 50ºC for 12 h to remove sorbed water. This was followed by the measurement of the dry weights (m_d) i.e., weight of chitosan membrane plus $AgNO_3$. These measurements allow the determination of $AgNO_3$ and water uptake in chitosan on a mass basis.

All sorption tests were carried out at room temperature, except for the experiments to study of the effect of temperatures. In this case, the solutions containing chitosan membranes were placed in an oven at the desired temperatures.

Chapter 4

Results and Discussion

4.1 Permeation Profile

In the permeation tests, the conductivity of the initially ion-free solution in the receptor compartment is measured as a function of time. A typical plot showing the conductivity data gathered at five-second intervals in a permeation test is presented in Fig. 4.1. The experimental conditions in this case were a feed $AgNO_3$ concentration of 0.07M, chitosan membrane thickness of 19μm and room temperature. As the de-ionized water obtained in the lab may contains a trace amount of ions, the initial receptor solution before diffusion of Ag^+ takes place sometimes has a small conductivity between 0 and 3μS/cm. The original conductivity of the de-ionized laboratory water is deducted from all conductivity data before correlation to the actual solution concentration.

Fig. 4.2 is the concentration profile corresponding to Fig. 4.1, obtained using a previously established calibration curve. (The calibration curve used in this study is presented in Appendix A.) Both of the transport parameters of Ag^+ in chitosan, diffusivity and permeability, are obtained from the concentration profiles in each permeation test. The first part of the diffusion process is the transient permeation, followed by steady state mass transfer. The steady state diffusion can be described by Eq. 2.9, and is indicated on the

overall concentration profile by the constant slope, representing constant permeation rate. The time lag τ as shown in Fig. 4.2 is obtained by extrapolating the steady state region of the curve back to zero concentrations. From transient permeation, diffusivity coefficient (D) is determined from τ using Eq. 2.10. From steady state permeation, permeance (P') and subsequently permeability coefficient (P) are obtained from the slope of the permeation curve using Eq. 2.4.

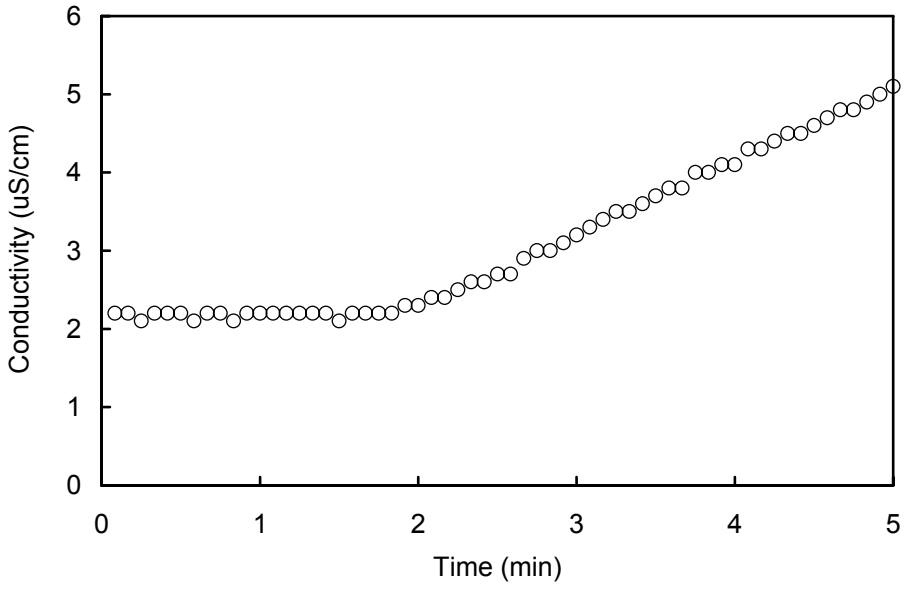

Figure 4.1 Time dependency of conductivity of the receptor solution, for diffusion of 0.07M $AgNO_3$ through a 19μm chitosan membrane at room temperature.

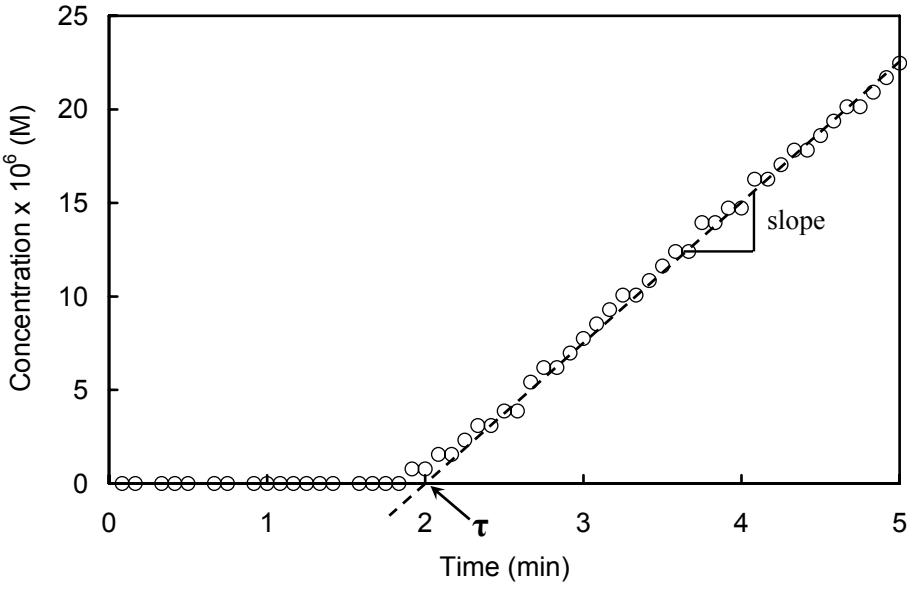

Figure 4.2 Time dependency of $AgNO_3$ concentration in the receptor compartment for the same experimental conditions as Fig. 4-1. τ is the time lag.

4.2 Membrane Thickness in Permeation

During the period between diffusing substances first entering the membrane and the time when a steady state of permeation is reached, the concentration at any point inside the membrane varies with time. Fig. 4.3 schematically demonstrates the change in the concentration profile across the membrane with permeation time. Prior to the permeation test, the membrane sample was stored in de-ionized water, and thus was swollen entirely by water. At the beginning of permeation, the water-swollen membrane was brought in contact with $AgNO_3$ solution on the feed side and water on the permeate side. $AgNO_3$ molecules started to be admitted from the side of the membrane in contact with the feed solution. The

silver concentration inside the membrane was therefore the highest at the surface contacting with the feed $AgNO_3$ solution, and the silver concentration was the lowest at the membrane surface on the permeate side. That is, a curved concentration profile along the membrane thickness is established, starting at the highest point inside the membrane surface of the feed side and gradually lowers towards the permeate side. As permeation approaches the steady state, more $AgNO_3$ molecules have been admitted into the membrane and the concentration profile gradually becomes more linear until the steady state when a straight profile across the membrane thickness is observed.

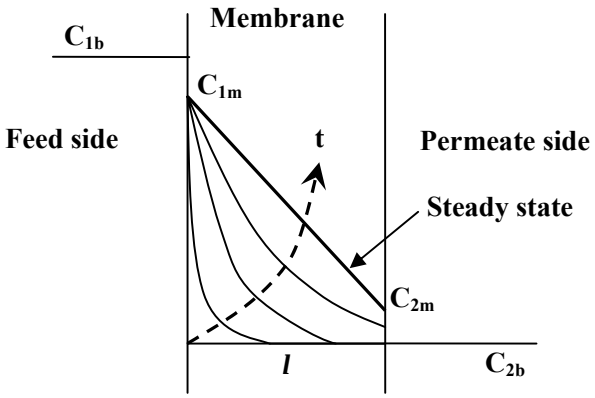

Figure 4.3 Schematic illustration of the concentration profile of permeate substances across the membrane during a permeation experiment.

As will be shown by the results from the sorption test, the membrane swells when immersed in the solution and to an extent determined by the solution concentration. This means that the membrane thickness is different between the transient state and the steady state of permeation, due to variation in the silver and water content inside the membrane. This deviation of membrane thickness should be taken into account for the determination of

the diffusivity and permeability coefficients. From the sorption experiments (refer to Section 4.3), a relationship is obtained between the original thickness of dry chitosan membrane and the actual thickness of the swollen membrane at sorption equilibrium:

$$R = \frac{l_w}{l_o} \tag{4.1}$$

where l_o is the original thickness of the dry chitosan membrane only; and l_w is the wet thickness when it is in sorption equilibrium with a $AgNO_3$ solution of known concentration. The ratio R of the two thicknesses, is obtained as a function of $AgNO_3$ concentration.

Determination of the diffusivity coefficient from the time lag is related to the transient state of permeation, a relatively short period after the start of permeation test. During the relatively short transient state, only a small amount of $AgNO_3$ was admitted into the membrane. The silver concentration inside the membrane is thus very low and the membrane is swollen due mostly to water. As a result, the thickness of Ag^+ free membrane was chosen for determination of the diffusivity coefficient. The membrane thickness used was thus corrected from the original thickness by the R value corresponding to zero concentration of $AgNO_3$. Unlike the diffusivity coefficient, the permeability coefficient is obtained from the permeation rate at the steady state. At this stage, the concentration profile of the solution inside the membrane is assumed to be linear. The membrane thickness used in determination of the permeability coefficient is therefore estimated by adjusting the original thickness by the average of the R values at zero concentration and the R values at the specific feed $AgNO_3$ concentration in the test.

4.3 Influence of Feed Concentration

4.3.1 Permeation

Permeation tests to determine the effect of feed $AgNO_3$ concentration were carried out under room temperature for membranes of three different thicknesses: 18, 20, and 26μm. These values of thicknesses are referred to the original thickness of a dry chitosan membrane before the permeation tests. The concentration dependency of the steady state permeation rate is shown in Fig. 4.4. The results obtained with three membranes with different thicknesses show similar trends of increasing permeation rate with concentration. This is expected as a larger concentration difference across the membrane means a larger driving force for permeation. Figs. 4.5 and 4.6 show the calculated permeance and permeability coefficients as a function of $AgNO_3$ concentration, respectively. The value of the permeability coefficient is obtained from the permeance by normalizing it with the membrane thickness estimated based on the feed concentration as described in Section 4.2. Both parameters increase with feed concentration from 0.08M before reaching a maximum at around 0.5-0.7M and then tend to decrease slightly at higher concentrations up to 1.0M. The effect of feed concentration on the permeability coefficient of silver ions in chitosan membrane has not been documented in the literature. Yet our results at low concentrations are similar to those of Du et al. [43] dealing with diffusion of K^+ in chitosan. They reported that the permeability increases with increasing feed K^+ concentration in the range of 0.001-0.1M.

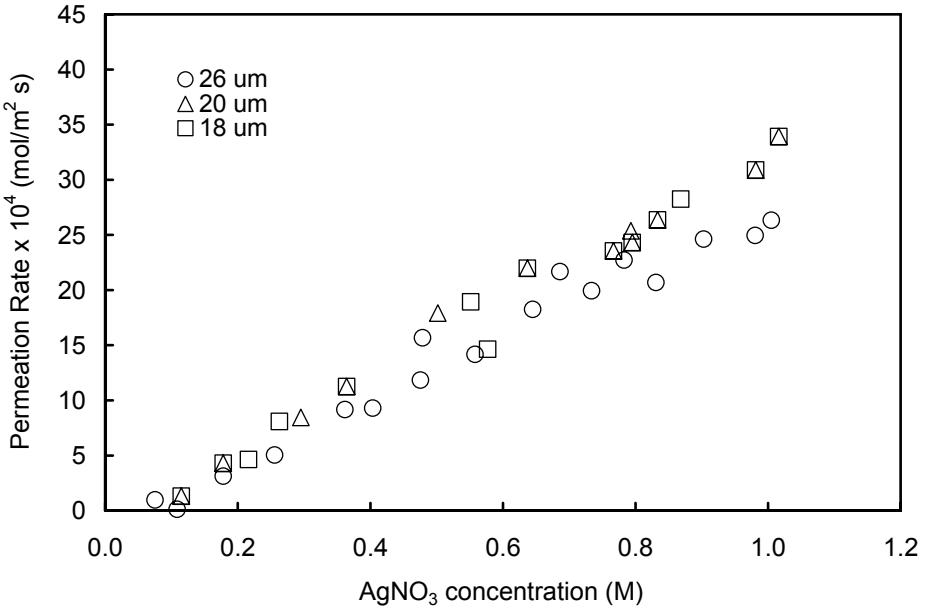

Figure 4.4 Effect of feed $AgNO_3$ concentration on the permeation rate of Ag^+ through chitosan membranes of thicknesses 16, 18, and 26 μm at room temperature.

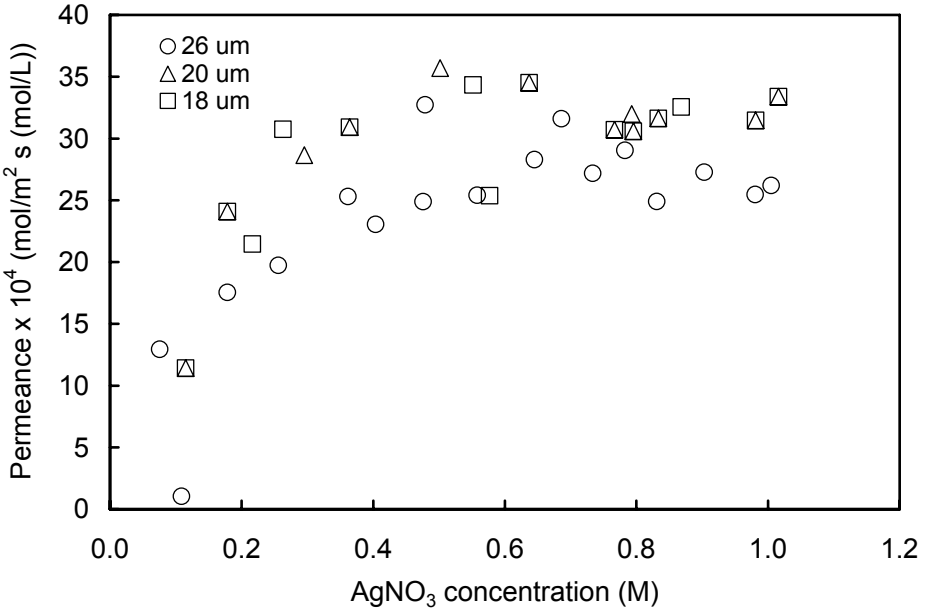

Figure 4.5 Effect of feed $AgNO_3$ concentration on the permeance of Ag^+ through chitosan membranes of thicknesses 16, 18, and 26 μm at room temperature.

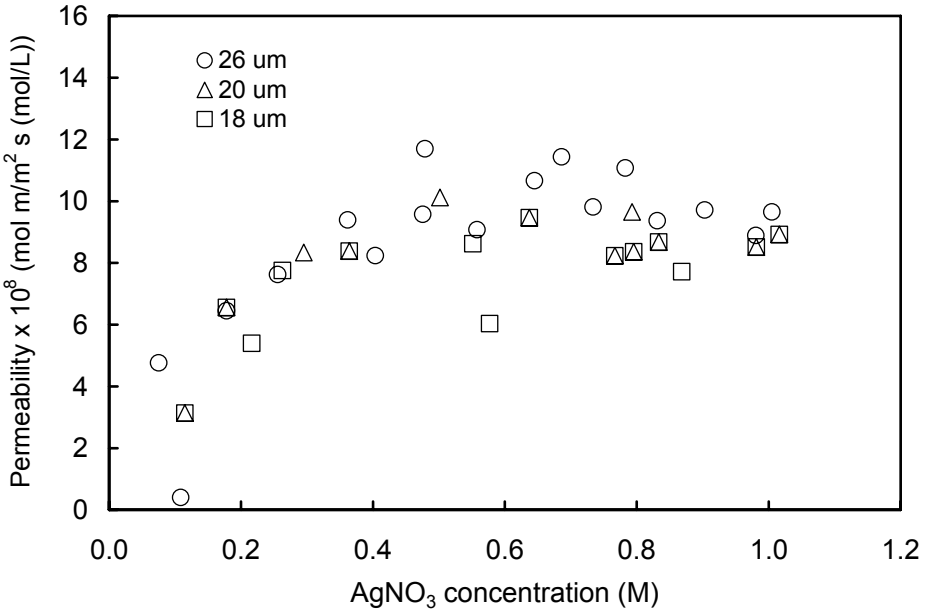

Figure 4.6 Effect of feed $AgNO_3$ concentration on the permeability of Ag^+ through chitosan membranes of thicknesses 16, 18, and 26 μm at room temperature.

The diffusivity coefficient, determined from the time lag using a membrane thickness based on the method described previously (i.e., water-swollen thickness), varies with concentration as presented in Fig. 4.7. Note that the equation used to calculate the diffusivity coefficient (Eq. 2.10) is derived from Fick's second law assuming that the diffusivity coefficient is constant with concentration. Our results show that the diffusivity coefficient of Ag^+ in chitosan is in fact a function of concentration. As a result, the diffusivity coefficient determined using the time lag can be considered to be the overall "apparent diffusivity". As will be shown later, the results from the sorption tests in combination with those from the permeation tests will allow the estimation of the diffusivity coefficient from the steady state

permeation rate (Eq.2.3). This will allow a comparison between the values obtained from the two methods, providing a deeper understanding of this parameter.

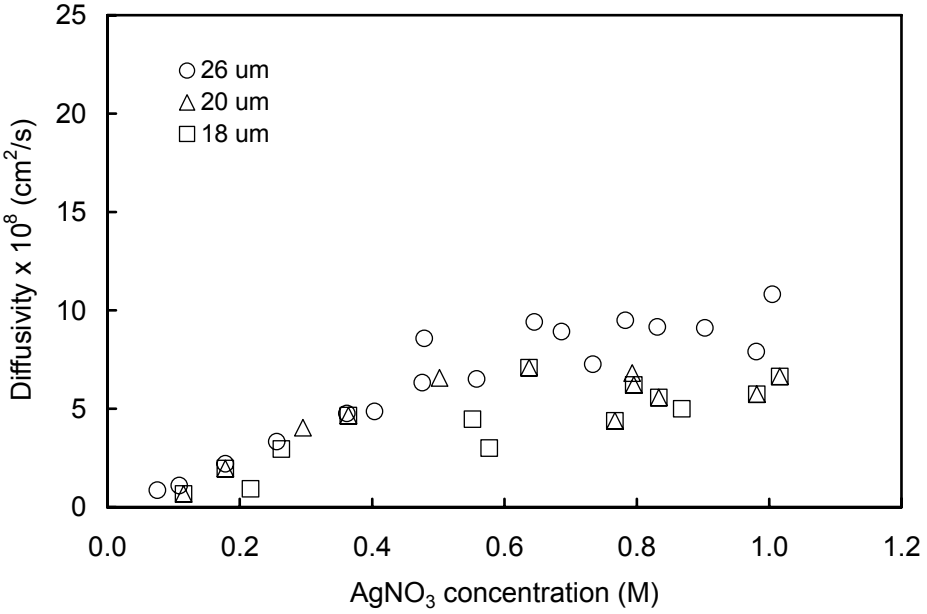

Figure 4.7 Effect of feed $AgNO_3$ concentration on the diffusivity coefficient of Ag^+ through chitosan membranes of thicknesses 16, 18, and 26 μm at room temperature. The diffusivity coefficient is evaluated from the time lag for transient permeation.

4.3.2 Sorption

The equilibrium sorption uptake of $AgNO_3$ for a concentration range of 0-1M and at room temperature is shown in Fig. 4.8 on a mass basis. The adsorption capacity of the adsorbate $AgNO_3$ in a chitosan membrane at equilibrium, q_e (mg/g), can be determined by:

$$q_e = \frac{m_d - m_o}{m_o} \times 1000 \qquad (4.2)$$

where m_o is the original weight of a dry chitosan membrane before adsorption (g), m_d is the dry weight of a dry chitosan membrane after adsorption (g). C_e (mg/L), the concentration of $AgNO_3$ in the liquid phase at equilibrium, is evaluated by:

$$C_e = C_0 - \frac{q_e m_o}{V} \tag{4.3}$$

where C_0 is the initial concentration of $AgNO_3$ in the solution (mg L^{-1}) and V is the volume of the $AgNO_3$ solution that remains relatively constant during the sorption experiments (mL).

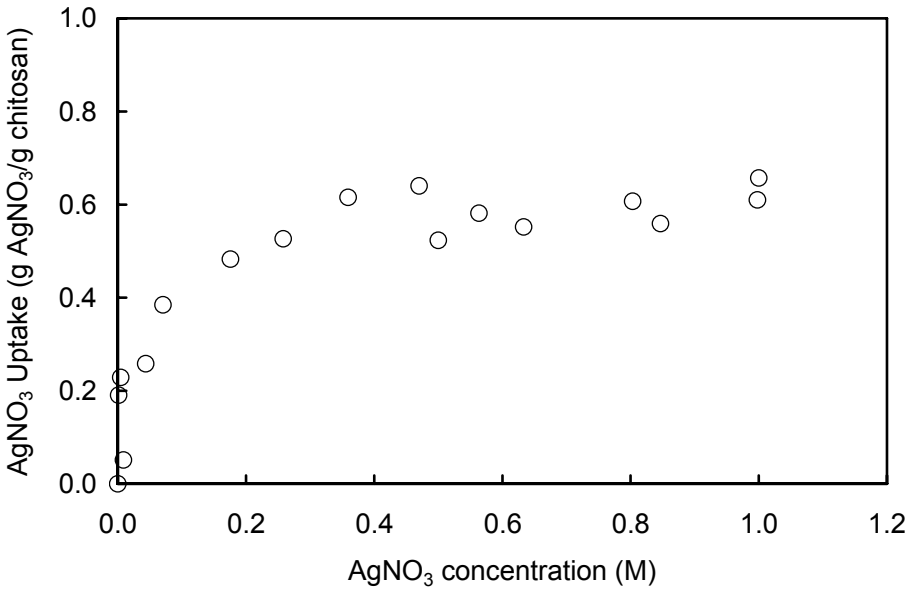

Figure 4.8 Effect of $AgNO_3$ concentration on sorption uptake of $AgNO_3$ in chitosan membranes at room temperature.

To evaluate the applicability of the Langmuir relationship, the plot of $\frac{C_e}{q_e}$ vs. C_e is prepared (Fig. 4.9), and a linear relationship is obtained with a correlation coefficient of 0.9875. This signifies compliance of adsorption of Ag^+ on chitosan with the Langmuir

isotherm. According to Eq. 2.18, the straight line has a slope of $\frac{1}{q_{\max}}$ and an intercept of $\frac{1}{q_{\max} b}$. Using linear regression, the values of $q_{\max}$ and b are determined to be 629 mg g^{-1} and 0.000148 L mg^{-1}, respectively.

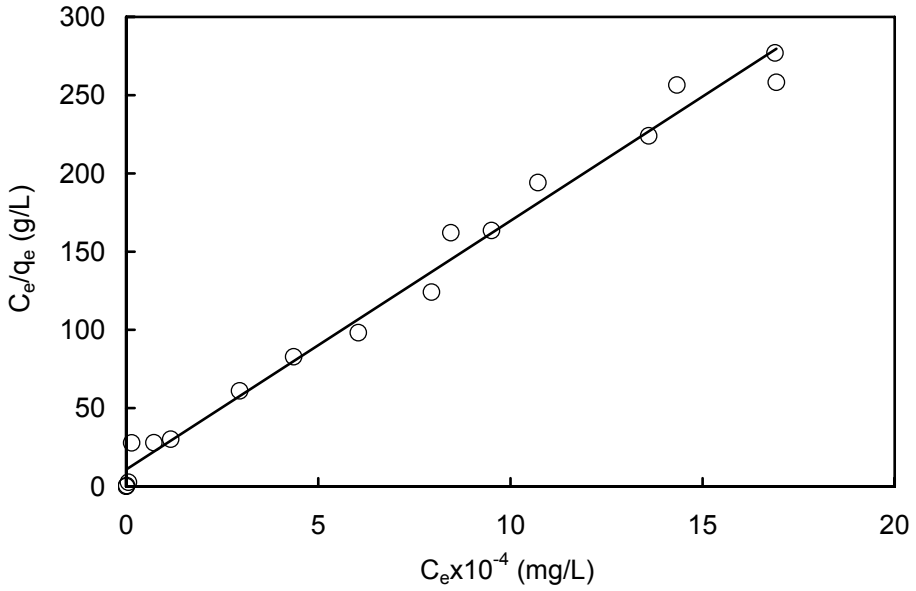

Figure 4.9 Adsorption isotherm of $AgNO_3$ in chitosan membranes, linearized according to the Langmuir equation.

In order to determine whether the Freundlich equation applies to the experimental sorption data (Eq. 2.20), q_e is plotted against C_e on a logarithmic scale (Fig. 4.10). It is found that the linear relationship is tremendously reduced in the mid to low concentration range, with a correlation coefficient of only 0.6443. This shows a relatively poor correlation with the Freundlich equation as compared to the Langmuir equation in the concentration range studied.

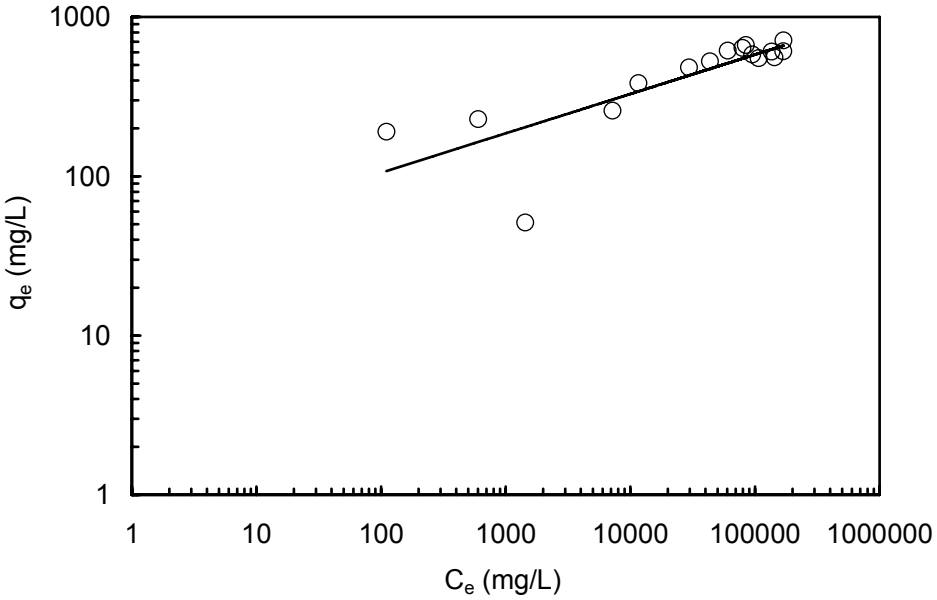

Figure 4.10 Adsorption isotherm of $AgNO_3$ in chitosan membranes, linearized according to the Freundlich equation.

Fig. 4.11 presents the trend of water uptake of the same membrane samples corresponding to the $AgNO_3$ uptake in Fig. 4.8,. At higher $AgNO_3$ solution concentrations, the uptake of water by chitosan substantially decreases. Generally speaking, both Ag^+ and water contents inside the membrane affect membrane swelling, and the degree of swelling is an overall contribution of the two effects. Because hydration of Ag^+ is limited, the contribution of the water content inside the membrane should be significant. Therefore, the degree of membrane swelling will decrease with increasing concentration of $AgNO_3$ due to lower concentration of water.

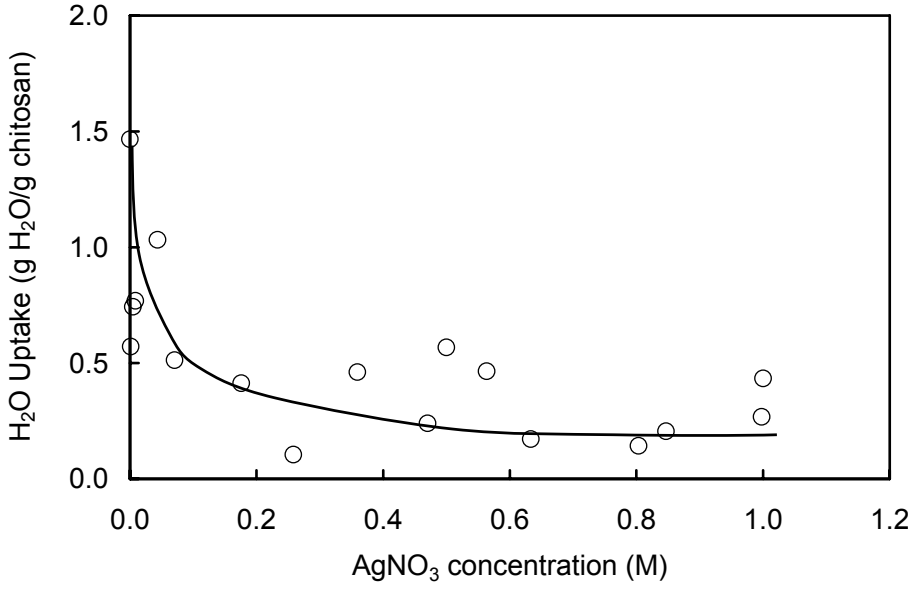

Figure 4.11 Effect of $AgNO_3$ concentration on sorption uptake of H_2O in chitosan membranes at room temperature.

When the sorption equilibrium is reached, the wet membrane thickness (l_w) was also measured. The intensity of membrane swelling is gauged by taking the ratio of the wet thickness at sorption equilibrium to the original thickness of dry chitosan membrane prior to the sorption test, as expressed by Eq. 4.1. This ratio R is determined at different $AgNO_3$ concentrations (Fig. 4.12). As expected, R decreases as the $AgNO_3$ concentration increases, representing a decrease in extent of membrane swelling that is related to amount of water and $AgNO_3$ uptake. Based on this information, the membrane thickness used for calculating the diffusivity and permeability coefficients from the transient and steady state of permeation, respectively, can be estimated, as discussed previously. The measurement of wet membrane

thickness also allows determination of the actual volume of chitosan membrane at sorption equilibrium for a given $AgNO_3$ concentration. Subsequently, the sorption uptake of $AgNO_3$ in chitosan on a mol per volume basis, corresponding to that on a mass basis, can be obtained (Fig. 4.13). These data will be used to evaluate the diffusivity coefficient from the steady state permeation rate (Eq. 2.3).

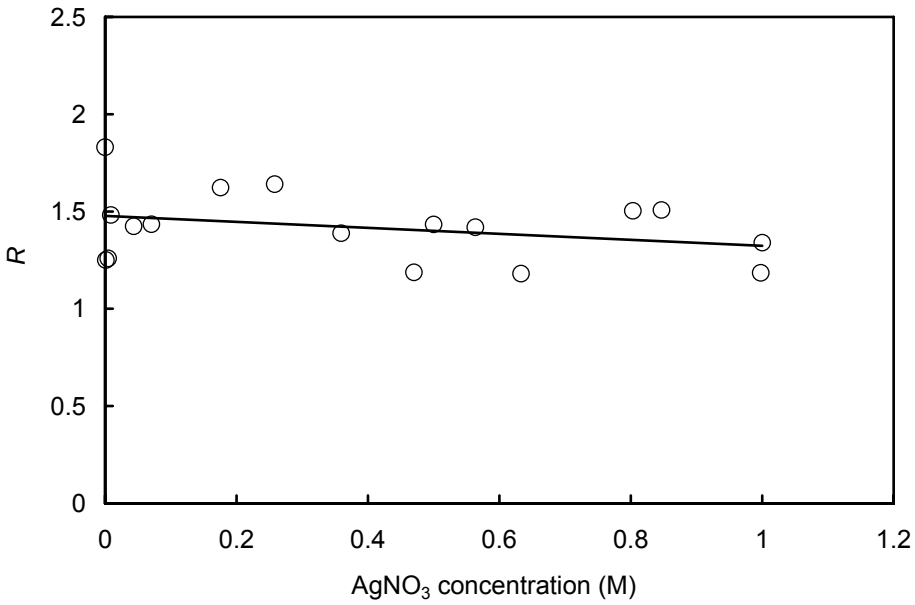

Figure 4.12 Effect of $AgNO_3$ concentration on the thickness of chitosan membrane at room temperature. *R* = wet membrane thickness at sorption equilibrium / original membrane thickness before sorption.

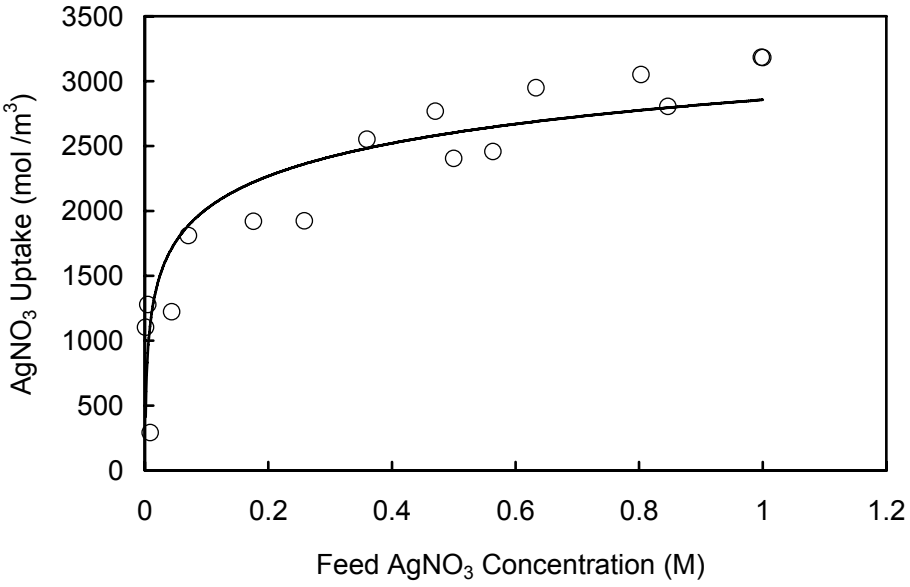

Figure 4.13 Effect of concentration on sorption uptake of $AgNO_3$ in chitosan membranes at room temperature (mol/ volume basis.)

4.4 Influence of Membrane Thickness

4.4.1 Permeation

The permeation tests to determine the effect of membrane thickness were carried out at room temperature with a feed $AgNO_3$ concentration of 1.0M. The membrane thicknesses used in the calculation for the permeability and diffusivity coefficients as well as those used for the x-axis of the plots presented in this section (Section 4.4.1) are the actual thickness of the swollen membrane estimated by the method described in Section 4.2. Fig. 4.14 shows a linear increase in the permeation rate with the inverse of the membrane thickness, as predicted by Fick's law and also in agreement with most physical processes including gas permeation through membranes [57,68]. The results for membrane thickness dependencies of permeance, permeability, and diffusivity are presented in Figs 4.15, 4.16, and 4.7, respectively. Their trends with membrane thickness in the concentration range tested are all in accordance with that shown in Figs 4.5 to 4.7. The diffusivity coefficient is usually constant for certain medium, pressure (in the case for gas diffusion), and temperature [51]. The result in Fig. 4.17, however, shows that the diffusivity coefficient tends to increase with membrane thickness. While the above implication of the diffusivity coefficient is usually only approximately true [51], there are other factors involved that complicate the diffusion process of Ag^+ in chitosan. One of these is associated with the chelating interaction between Ag^+ and chitosan. The transport process includes both adsorption and diffusion of Ag^+ and accompanying anions through the membrane. During the transport process, the amino and hydroxyl groups on the surface of the chitosan membrane have the ability to form chitosan-

Ag^+ complexes (chelating). This may happen before, after, or together with the diffusion of $AgNO_3$ through the membrane and may influence the entire permeation process. Therefore, the chemical interaction between chitosan and Ag^+ is expected to affect the diffusivity and permeability parameters. In addition, the local Ag^+ concentration varies from point to point along the membrane thickness due to a non-uniform concentration profile. The difference in concentration and the subsequent difference in the degree of membrane swelling result in different local diffusivities. As a consequence of the factors that are involved in the permeation of Ag^+ in chitosan, the values of the permeation properties determined from the experiments are in fact the overall apparent properties.

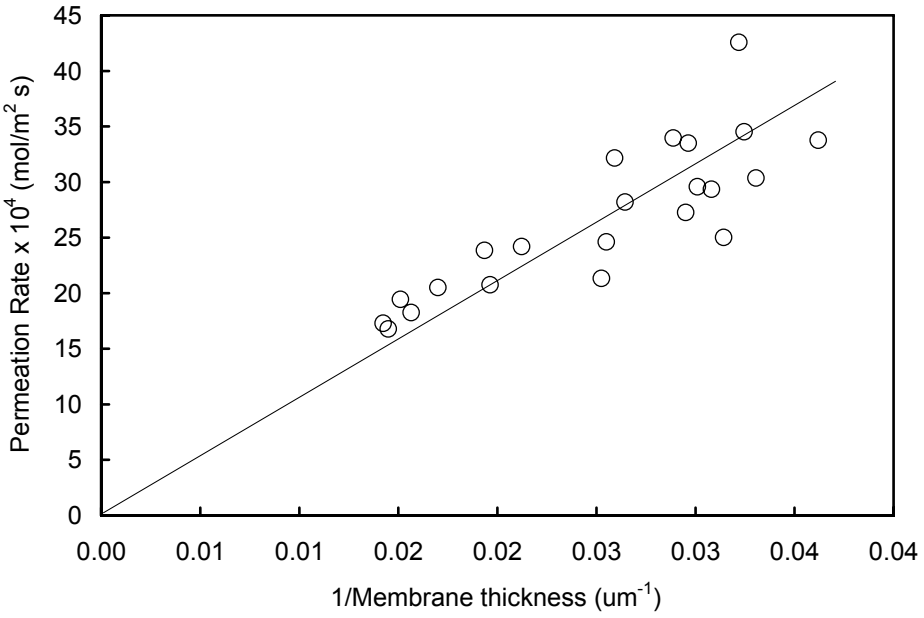

Figure 4.14 Effect of membrane thickness on permeation rate of Ag^+ for feed $AgNO_3$ concentration of 1.0M at room temperature.

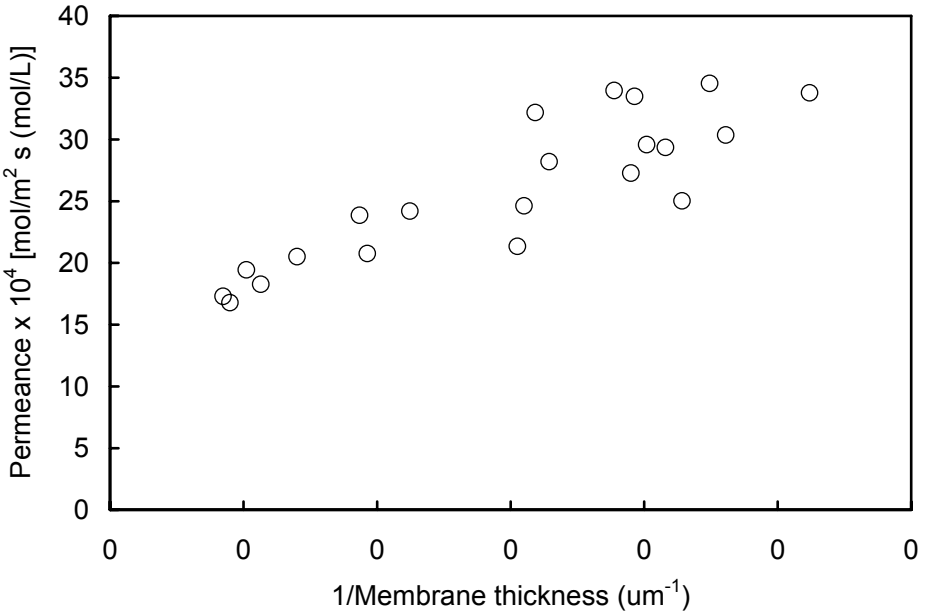

Figure 4.15 Effect of membrane thickness on permeance of Ag^+ for feed $AgNO_3$ concentration of 1.0M at room temperature.

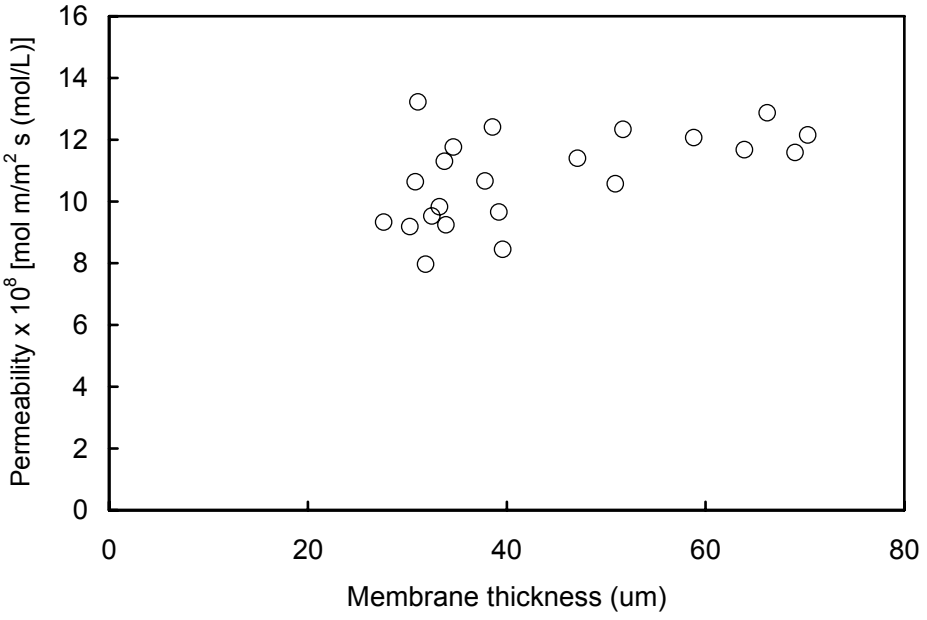

Figure 4.16 Effect of membrane thickness on permeability of Ag^+ for feed $AgNO_3$ concentration of 1.0M at room temperature.

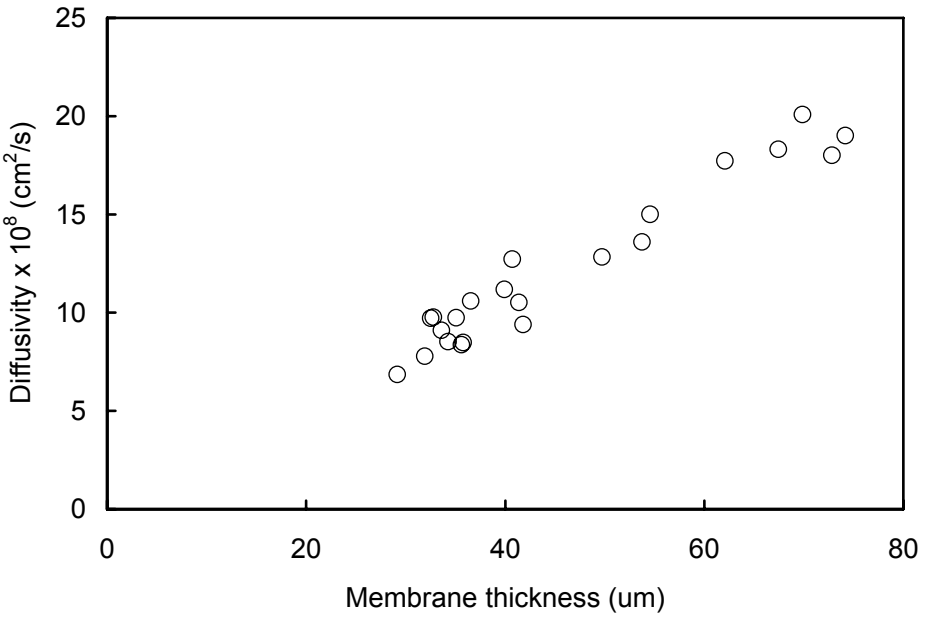

Figure 4.17 Effect of membrane thickness on diffusivity of Ag^+ for feed $AgNO_3$ concentration of 1.0M at room temperature.

There have been studies on the adsorption of metal ions on solid particles, a process that involves the steps of external diffusion, internal diffusion within chitosan, and uptake of ions on the interior sites via chemical complexation [6,61,62,69]. Table 4.1 summarizes the studies that have investigated chitosan as sorbent for metal ions and the suggested rate controlling step. It can be seen that external diffusion is rarely rate determining. While there is no uniform agreement in whether chemical complexation or internal diffusion is rate controlling, the results do show that chemical complexation definitely plays a role in the adsorption process.

It is clear that at the present stage, the exact mechanisms of permeation involving chemical complexation/chelation of metal ions on chitosan are unknown. Nevertheless, the

role of chelation and its influence on ionic permeation is ineligible, making the permeation process of Ag^+ in chitosan more than simple Fickian diffusion.

Table 4.1 Results in different studies regarding rate determining step in adsorption process

Adsorbate	Adsorbent	Rate controlling step	Reference
Cd(II)	Chitosan	Diffusion	[6]
Cu(II), Pb(II), Cr(VI)	Chitosan	Diffusion	[61]
Fe(II), Fe(III)	Chitosan	Chemical complexation	[62]
Cr(VI), Cu(II)	Chitosan	Chemical complexation	[69]

4.4.2 Sorption

The effect of membrane thickness on $AgNO_3$ uptake in chitosan at room temperature is given by Fig. 4.18. The membrane thickness on the x-axis is referred to the original thickness prior to sorption. The results show that the sorption uptake of $AgNO_3$ in chitosan membrane is independent of membrane thickness for both concentrations tested, indicating that the sorption occurs in the bulk of the polymer as opposed to just on the surface. The corresponding water uptake shows no dependency on the membrane thickness either (Fig. 4.19).

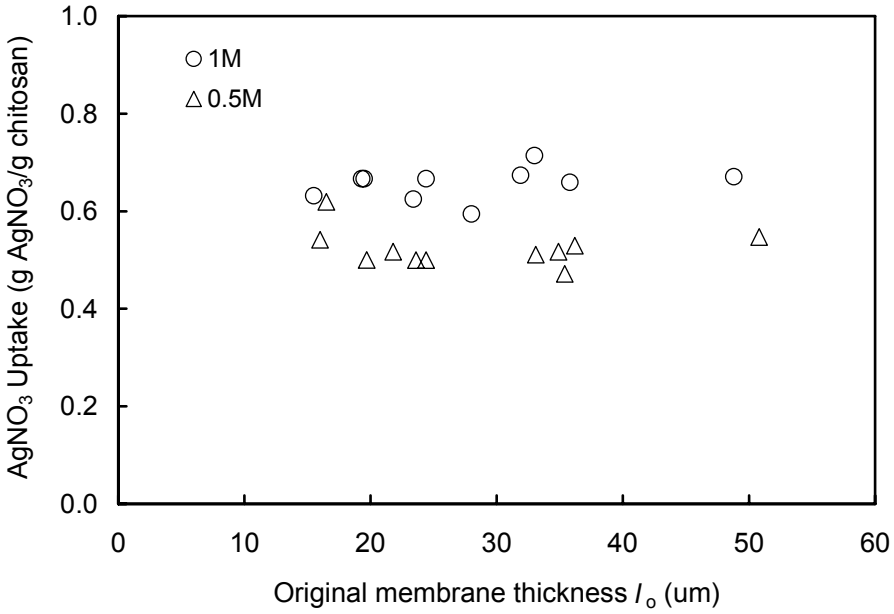

Figure 4.18 Sorption uptake of $AgNO_3$ in chitosan membranes for $AgNO_3$ concentrations of 1.0 and 0.5M at room temperature.

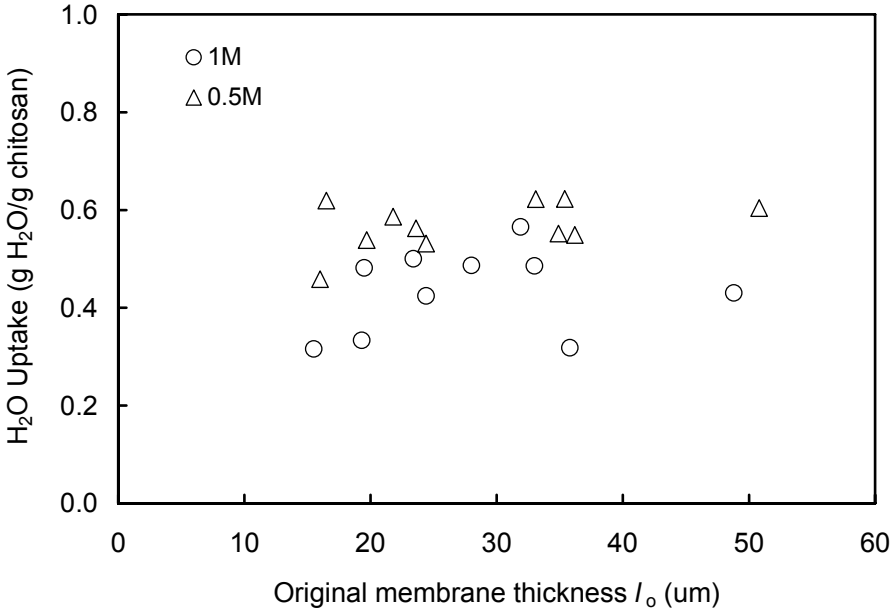

Figure 4.19 Sorption uptake of H_2O in chitosan membranes for $AgNO_3$ concentrations of 1.0 and 0.5M at room temperature.

4.5 Influence of Operating Temperature

4.5.1 Permeation

Fig. 4.20 displays the effect of temperature on the $AgNO_3$ permeation rate at a feed $AgNO_3$ concentration of 1M through chitosan membranes of 21μm thick. The increase in the permeation rate with temperature is expected according to the free volume theory [70], which states that the thermal motion of polymer chains randomly produces free volumes. As temperature rises, the frequency of the polymer chain motion increases resulting in a larger free volume and thus a higher permeation rate. An increase in the mobility of Ag^+ with temperature may also be another contributing factor of increasing permeation rate with temperature.

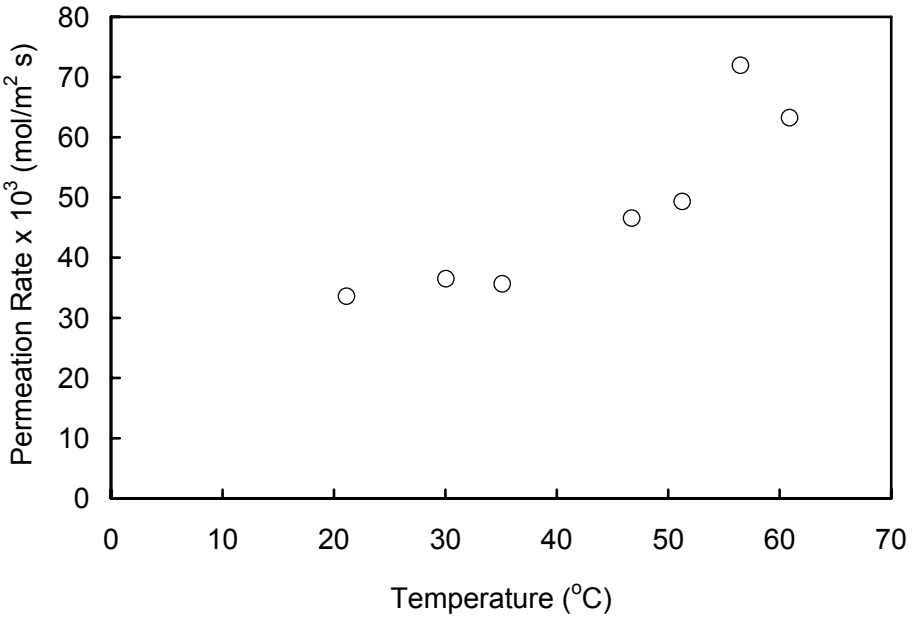

Figure 4.20 Effect of operating temperature on permeation rate of Ag^+ through chitosan membrane of 21μm and for feed $AgNO_3$ concentration of 1.0M.

The values of permeance, permeability coefficient, and diffusivity coefficient at different temperatures are summarized in Table 4.2. To analyze the temperature dependencies of the permeability and diffusivity coefficients, the Arrhenius equation was used (Eqs. 2.13-2.14). The plots showing permeability and diffusivity coefficients versus the reciprocal of temperature on a semi-log scale are demonstrated in Figs. 4.21 and 4.22, respectively. In both cases, linear relationships are obtained, indicating the Arrhenius relationships are followed. A least square fit to the experimental data is used to determine the activation energies for permeation (E_p) and diffusion (E_d), which are shown in Table 4.3. With the calculated values of E_p and E_d, the heat of sorption is determined using Eq. 2.15 and is also shown in Table 4.3.

Table 4.2 Permeance (P'), permeability coefficient (P) and diffusivity coefficient (D) values of Ag+ in chitosan membrane at different temperatures [a]

Temperature (^oC)	P' x 10^4 [mol/m^2 s (mol/L)]	P x 10^8 {mol m/[m^2 s (mol/L)]}	D x 10^8 (cm^2/s)
21	33.6	10.2	6.9
30	36.5	10.8	6.4
35	35.6	11.2	7.8
47	46.5	13.2	8.6
51	49.3	14.6	10.2
56	71.9	19.6	9.8
61	63.2	17.8	9.0

[a] Feed $AgNO_3$ concentration 1.0M, membrane thickness 21μm.

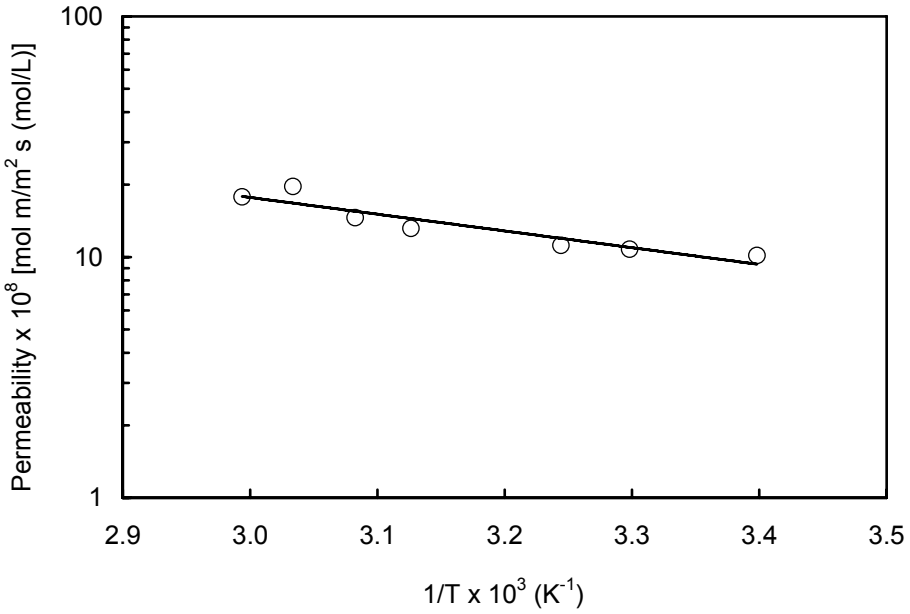

Figure 4.21 Effect of operating temperature (T) on permeability of Ag^+ through chitosan membrane. Feed $AgNO_3$ concentration 1.0M, membrane thickness 21μm.

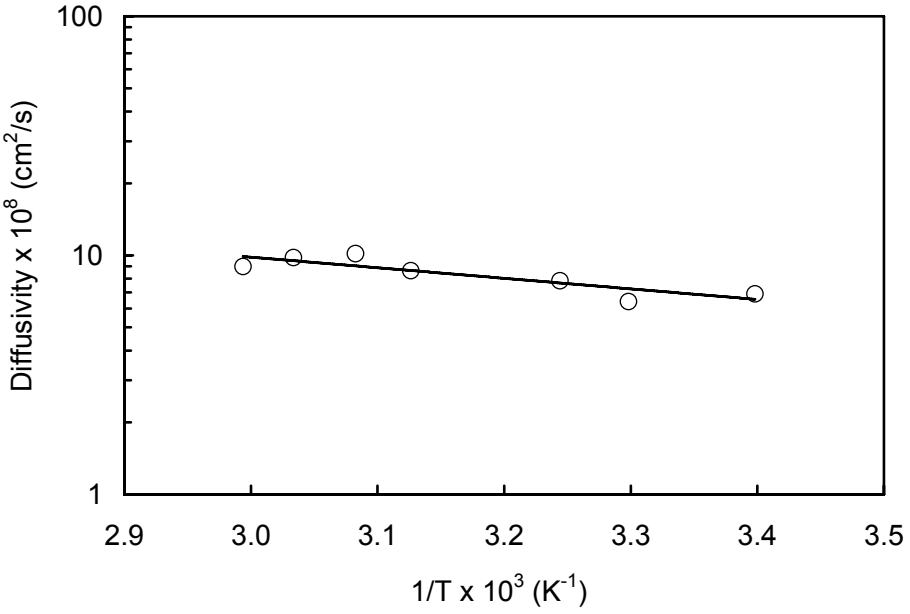

Figure 4.22 Effect of operating temperature (T) on diffusivity of Ag^+ through chitosan membrane. Feed $AgNO_3$ concentration 1.0M, membrane thickness 21μm.

Table 4.3 Activation energies for permeation (E_p) and diffusion (E_d) and the heat of sorption (ΔH_s) for Ag+ in chitosan membrane

Arrhenius activation parameters	
E_p (kJ/mol)	13.3
E_d (kJ/mol)	8.5
ΔH_s (kJ/mol)	4.8

4.5.2 Sorption

The value of ΔH_s is positive (Table 4.3), suggesting that the sorption of Ag^+ on chitosan is an endothermic process. The actual sorption data presented in Fig. 4.23, however, do not exhibit an evident trend, probably due to the weak endothermic sorption process as suggested by the small value of ΔH_s. Likewise, the water uptake displayed in Fig. 4.24 does not provide a clear picture either. It is recommended that more work be conducted on this regard in the future.

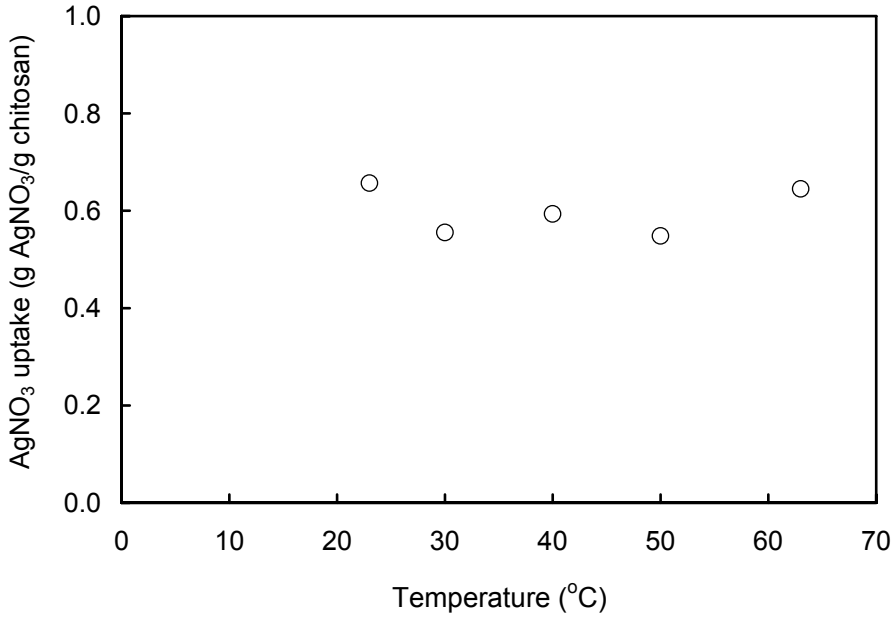

Figure 4.23 Sorption uptake of $AgNO_3$ in chitosan membrane at different temperatures and at an $AgNO_3$ concentration of 1.0M.

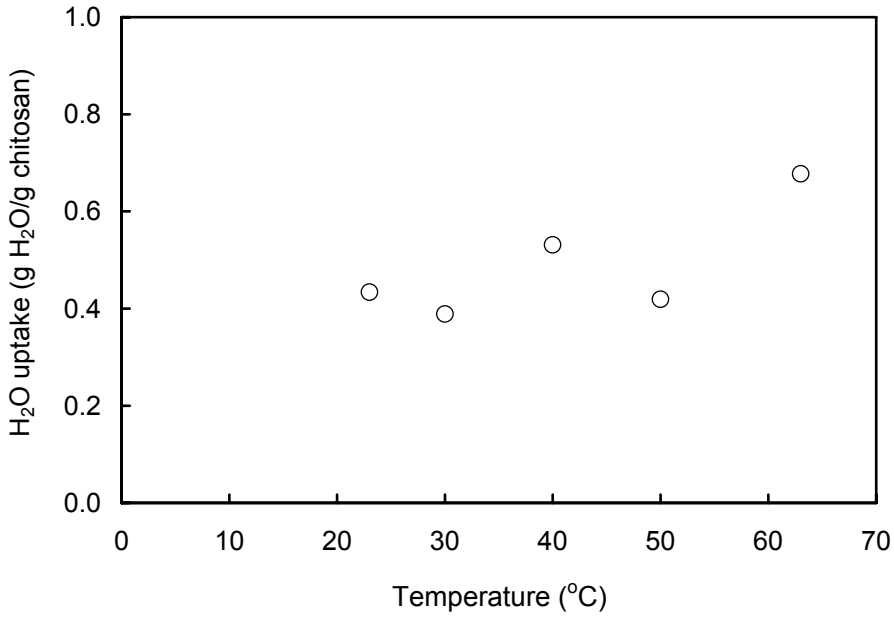

Figure 4.24 Sorption uptake of H_2O in chitosan membrane at different temperatures and at an $AgNO_3$ concentration of 1.0M.

Membrane swelling was also studied at different temperatures. As shown in Fig. 4.25, the temperature has very little influence in the range tested. This result is no surprise as swelling is related to water and $AgNO_3$ uptake. No evident effect of temperature on the membrane swelling is observed. This is in agreement with the data in Figs. 4.23 and 4.24, where silver uptake and water uptake are only affected by the temperature slightly.

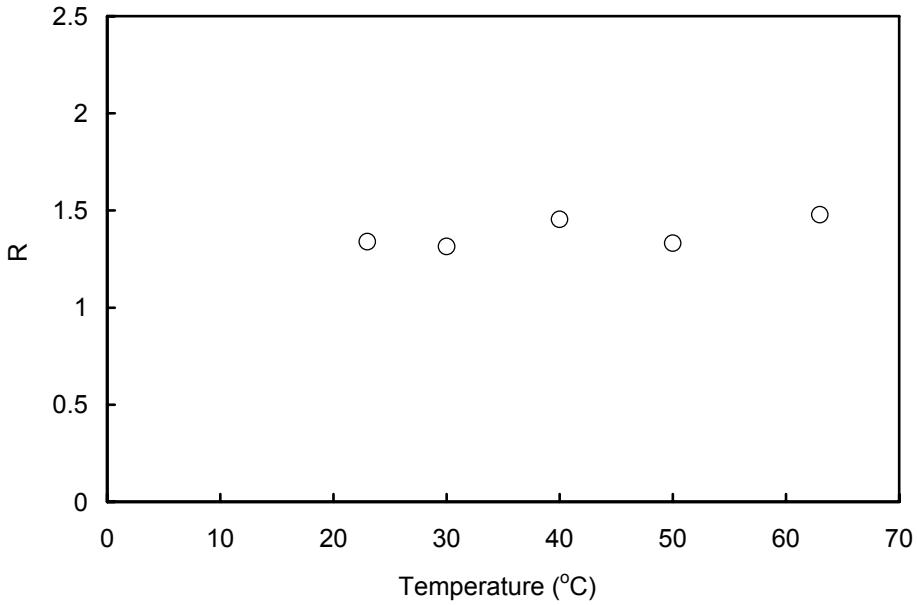

Figure 4.25 Effect of operating temperature on thickness of chitosan membranes. R = wet membrane thickness at sorption equilibrium / original membrane thickness before sorption.

4.6 Diffusivity Coefficient from the Steady State Permeation Rate

Determination of the diffusivity coefficient from the steady state permeation rate using Eq. 2.3 is not feasible when the concentrations at the membrane surface are not readily known. Nevertheless, with the results from the sorption tests of this study, information required to determine the diffusivity coefficient from Eq. 2.3 can be obtained. Fig. 4.13 shows the equilibrium concentration of silver within the chitosan membrane at different concentrations of $AgNO_3$ solution. At the steady state, the membrane surface on the upstream side is in equilibrium with the feed solution. Therefore, the relationship in Fig. 4.13 can be used to estimate C_{1m} for a given feed $AgNO_3$ concentration. C_{2m}, the concentration of Ag^+ at the membrane surface on the permeate side can be assumed to be negligible. This assumption is based on the fact of the extremely dilute condition in the receptor compartment ($<10^{-3}$M) as a result of constant stirring and its relatively large volume compared to that of the feed. The diffusivity coefficient can then be estimated based on steady state Fickian permeation using Eq. 2.3. The membrane thickness used in this calculation is the estimated thickness at the steady state, which is essentially the same as that used in the determination of the permeability coefficient.

Figs. 4.26-4.28 show a comparison between the values of the diffusivity coefficient determined by the time lag method and by the steady state permeation rate at different feed concentrations, membrane thicknesses, and operating temperatures, respectively. It is shown that the values obtained from both methods show very similar trends with feed concentration. The values obtained from the steady state of permeation are nonetheless much larger than

that from the time lag method. This difference can be attributed to the fact that the diffusivity coefficients are determined during different stages of diffusion. The diffusivity coefficient determined using Eq. 2.3 corresponds to the steady state permeation data when a linear concentration profile is established; while that determined using the time lag corresponds to the initial transient state of permeation. In the stage of permeation before steady state is reached, the Ag^+ concentration inside the membrane is lower, thus reducing the diffusivity (Fig.4.3). Another possible factor contributing to the difference is the chelating interactions between Ag^+ and chitosan that result in the formation of chitosan-metal complexes. During the transient state when the Ag^+ concentration is low, most Ag^+ entering the membrane may tend to form complexes and as a result their mobility within the membrane is restricted. When Ag^+ concentration rises as the steady state is approached, most complexing sites in chitosan may be occupied. Therefore, Ag^+ ions admitted into the membrane will be able to freely diffuse in the membrane, resulting in a higher diffusivity.

The transient state of permeation is relatively short period in the permeation process. As most applications of chitosan involving Ag^+ are related to steady state of permeation, the diffusivity values obtained from the steady state permeation rate would be more relevant from the application point of view.

a)

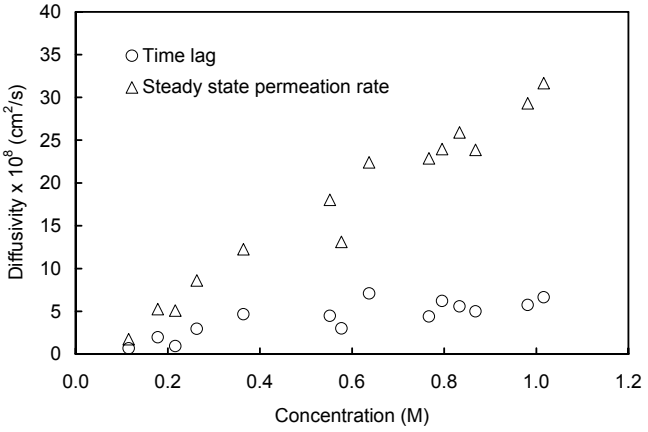

b)

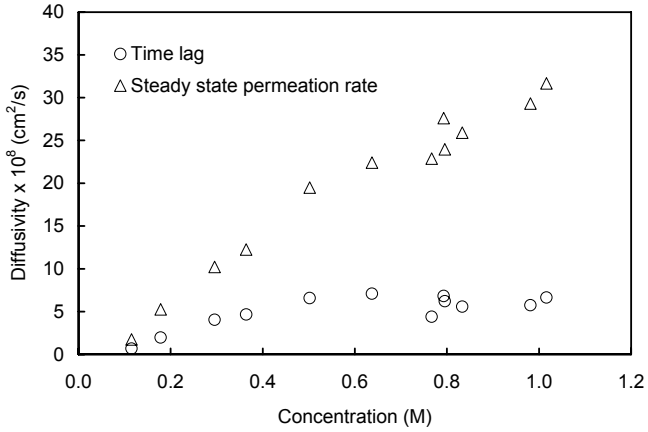

c)

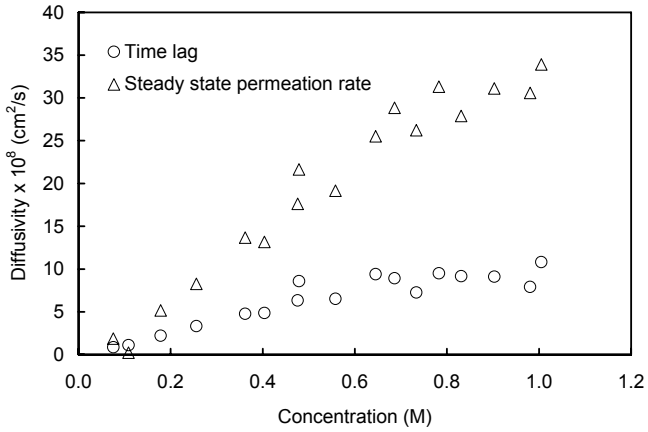

Figure 4.26 Comparison of diffusivity coefficients determined by time lag and from by Eq. 2.3 for different $AgNO_3$ feed concentrations. Membrane thickness (original thickness l_o): a) 18μm b) 20μm c) 26μm, room temperature.

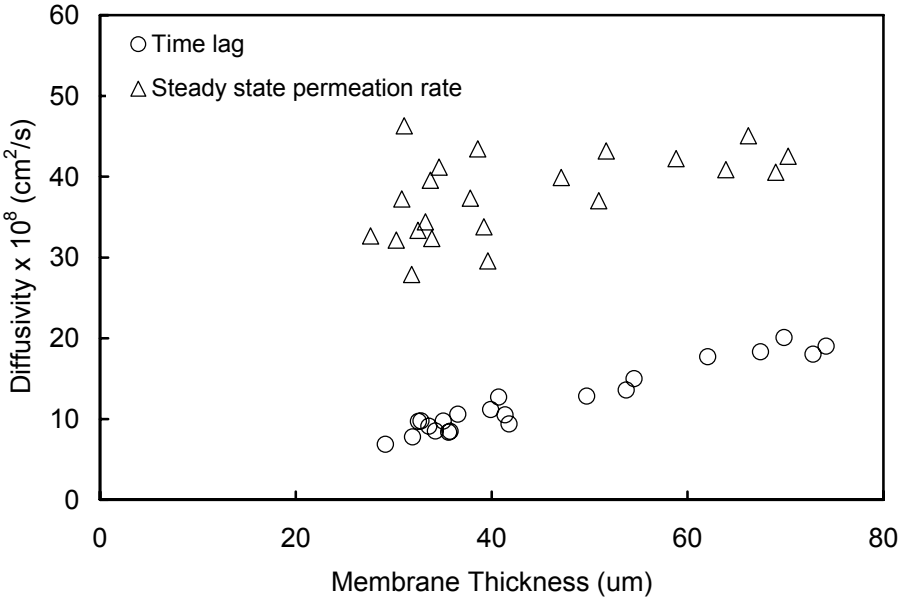

Figure 4.27 Comparison of diffusivity coefficients determined by time lag and by Eq. 2.3 for different membrane thicknesses (actual thickness at transient state for time lag method, and actual thickness at steady state for Fick's law). Feed $AgNO_3$ concentration 1.0M, room temperature.

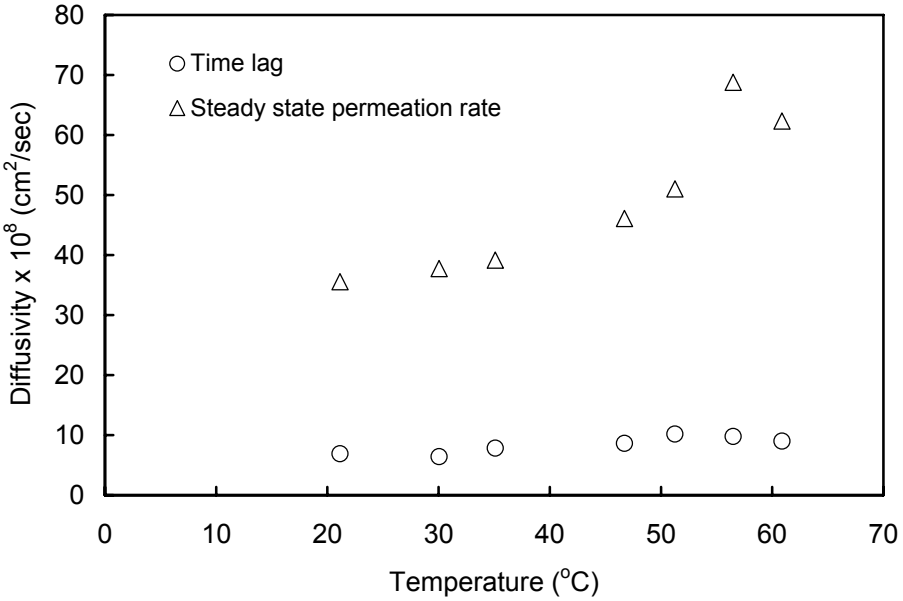

Figure 4.28 Comparison of diffusivity coefficients determined by time lag and by Eq. 2.3 at operating temperatures. Feed $AgNO_3$ concentration 1.0M, membrane thickness 21μm.

Chapter 5

Conclusions and Recommendations

5.1 Conclusions

The diffusivity of Ag^+ in chitosan was studied using the time lag method and steady state permeation. The diffusivity coefficient was found to be concentration dependent, and the diffusivity evaluated was the overall "apparent diffusivity". The diffusivity coefficient also varied with operating temperature, and the temperature dependency followed the Arrhenius trends.

The sorption of Ag^+ in chitosan appeared to be a slightly endothermic process. The sorption uptake was shown to take place mainly in the bulk of chitosan membrane, and the sorption isotherm could be described by the Langmuir equation. The maximum adsorption capacity was determined to be 629mg/g at room temperature.

The swelling of chitosan was related to the Ag^+ and water sorption uptake. The degree of swelling tended to decrease with an increase in $AgNO_3$ concentration, but the operating temperature did not appear to affect swelling significantly.

The chelating interactions between Ag^+ and chitosan had an impact on the transport properties of Ag^+. In addition, as the diffusivity coefficient is dependent on concentration, the permeation process is not a mere Fickian diffusion with constant diffusivity.

The diffusivity coefficients determined by the time lag method and from the steady state permeation rate were found to display similar trends with the variables investigated: $AgNO_3$ concentration, membrane thickness, and temperature. The differences in values obtained by the two methods were attributed to the different stages of permeation (i.e., the transient permeation in the initial stage and the steady state permeation in the later stage). In addition, the Ag^+-chitosan interaction caused by the chelating properties of chitosan was another factor that affected the mobility of Ag^+ during transient and steady state permeation.

5.2 Recommendations

The following are recommended as an extension of this work to provide further insight into transport of Ag^+ in chitosan.

- In the present study, the sorption tests were carried out at a narrow temperature range from room temperature to 63^oC, and the heat of sorption determined was not substantially different from zero. It is recommended that sorption tests be carried out at a wider temperature range so as to confirm endothermic or exothermic sorption of Ag^+ in chitosan.
- Investigations on the rate of Ag^+ uptake in chitosan membrane should be carried out to determine the permeation mechanism of the Ag^+ mobility in chitosan membranes. If the rate of adsorption is dependent on the membrane thickness, the permeation of Ag^+ in chitosan would be diffusion controlled. Otherwise, the permeation would be reaction controlled.

- Different silver salts can be utilized for the permeation and sorption tests to determine the effect of anions in the silver salts on transport of Ag^+ in chitosan.

References

[1] Herrera PS, Feng X, Payzant JD, Kim JH. Process for the Separation of Olefins from Paraffins Using Membranes. Canadian Patent CA 2426629.

[2] Mi F, Wu Y, Shyu S, Chao A, Lai J, and Su C. Asymmetric chitosan membranes prepared by dry/wet phase separation: a new type of wound dressing for controlled antibacterial release. Journal of Membrane Science 2003; 212:237-254.

[3] Mi F, Wu Y, Shyu S, Schoung J, Huang Y, Tsai Y, and Hao J. Control of wound infections using a bilayer chitosan wound dressing with sustainable antibiotic delivery. Journal of Biomedial Materials Research 2002; 59(3):438-449.

[4] Lasko CL, Hurst MP. An investigation into the use of chitosan for the removal of soluble silver from industrial wastewater. Environmental Science & Technology 1999; 33(20):3622-2626.

[5] Katarina RK, Takayanagi T, Oshima M, Motomizu S. Synthesis of a chitosan-based chelating resin and its application to the selective concentration and ultratrace determination of silver in environmental water samples. Analytica Chimica Acta 2006; 558(1-2):246-253.

[6] Evans JR, Davids WG, MacRae JD, Amirbahman A. Kinetics of cadmium uptake by chitosan-based crab shells. Water Research 2002: 36:3219-3226.

[7] Masri MS, Reuter FW, Friedman M. Binding of metal cations by natural substances. Journal of Applied Polymer Science 1974; 18:675-681.

[8] Tharanathan RN, Kittur FS. Chitin – the undisputed biomolecule of great potential. Critical Reviews in Food Science and Nutrition 2003; 43(1):61-87.

[9] Kurita K. Controlled functionalization of the polysaccharide chitin. Progress in Polymer Science 2001; 26:1921-1971.

[10] Pangburn SH, Trescony PV, Heller J. Partially Deacetylated Chitin: Its Use in Self-Regulated Drug Delivery Systems. In: Zikakis JP (Ed.). Chitin, Chitosan, and Related Enzymes. Orlando: Academic Press; 1984. p.3-19.

[11] Krajewska B. Application of chitin-and chitosan-based materials for enzyme immobilizations: a review. Enzyme and Microbial Technology 2004; 35:126-139.

[12] Hirano S, Senda H, Yamamoto Y, Watanabe A. Several Novel Attempts for the Use of the Potential Functions of Chitin and Chitosan. In: Zikakis JP. Chitin, Chitosan, and Related Enzymes. Orlando: Academic Press; 1984. p.77-95.

[13] Krajewska B. Diffusion of metal ions through gel chitosan membranes. Reactive & Functional Polymers 2001; 47:37-47.

[14] Davis B, Eveleigh DE. Chitosanases: Occurance, Production and Immobilization. In: Zikakis JP (Ed.). Chitin, Chitosan, and Related Enzymes. Orlando: Academic Press; 1984. p.161-179.

[15] Muzzarelli RAA. Natural Chelating Polymers. New York: Pergamon Press; 1973.

[16] McCormick CL, Anderson KW. Synthesis and Characterization of Chitin Pendently Substituted with the Herbicide Metribuzin. In: Zikakis JP (Ed.). Chitin, Chitosan, and Related Enzymes. Orlando: Academic Press; 1984. p.42-53.

[17] Spreen KA, Zikakis JP, Austin PR. The Effect of Chitinous Materials on the Intestinal Microflora and the Utilization of Whey in Monogastric Animals. In: Zikakis JP (Ed.). Chitin, Chitosan, and Related Enzymes. Orlando: Academic Press; 1984. p.57-75.

[18] Sandford PA. Chitosan: Commercial Uses and Potential Applications. In: Skjak-Braek G, Anthonsen T, Sandford P. Chitin and Chitosan – Sources, Chemistry, Biochemistry, Physical Properties and Applications. London: Elsevier Applied Science; 1989. p.51-69.

[19] Brine CJ. Introduction Chitin: Accomplishments and Perspectives. In: Zikakis JP. Chitin, Chitosan, and Related Enzymes. Orlando: Academic Press; 1984.

[20] Hudson SM, Smith C. Polysaccharides: chitin and chitosan: chemistry and technology of their use as structural materials. In: Kaplan DL (Ed.). Biopolymers from Renewable Resources. Berlin: Springer-Verlag;1998. p.96-118.

[21] Muzzarelli RAA. Chitin. Oxford: Pergamon Press; 1977.

[22] Dutta PK, Rayikumar MNV, Dutta J. Chitin and chitosan for versatile applications. Journal of Macromolecular Science 2002; C42(3):307-354.

[23] Ham-Pichavant F, Sebe G, Pardon P, Coma V. Fat resistance properties of chitosan-based paper packaging for food applications 2005; 61:259-265.

[24] Qin Y, Zhu C, Chen J, Chen Y, and Zhang C. The absorption and release of silver and zinc ions by chitosan fibers. Journal of Applied Polymer Science 2006; 101:766-771.

[25] Allan GG, Altman LC, Bensinger RE, Ghosh DK, Hirabayashi Y, Neogi AN, Neogi S. Biomedical Applications of Chitin and Chitosan. In: Zikakis JP (Ed.). Chitin, Chitosan, and Related Enzymes. Orlando: Academic Press; 1984. p.119-133.

[26] Brine CJ. Controlled Release Pharmaceutical Applications of Chitosan. In: Skjak-Braek G, Anthonsen T, Sandford P (Eds.). Chitin and Chitosan – Sources, Chemistry, Biochemistry, Physical Properties and Applications. London: Elsevier Applied Science; 1989. p.679-691.

[27] Nagai T, Sawayanagi Y, Nambu N. Application of Chitin and Chitosan to Pharmaceutical Preparations. In: Zikakis JP (Ed.). Chitin, Chitosan, and Related Enzymes. Orlando: Academic Press; 1984. p.21-39.

[28] Markey ML, Bowman LM, Bergamini MVW. Contact Lenses Made of Chitosan. In: Skjak-Braek G, Anthonsen T, Sandford P (Eds.). Chitin and Chitosan – Sources, Chemistry, Biochemistry, Physical Properties and Applications. London: Elsevier Applied Science; 1989. p.713-717.

[29] Hadwiger, LA, Fristensky B, Riggleman RC. Chitosan, A Natural Regulator in Plant-Fungal Pathogen Interactions, Increases Crop Yields. In: Zikakis JP (Ed.). Chitin, Chitosan, and Related Enzymes. Orlando: Academic Press; 1984. p.291-302.

[30] Svang-Ariyaskul A, Huang RYM, Douglas PL, Pal R, Feng X, Chen P, Liu L. Blended chitosan and polyvinyl alcohol membranes for the pervaporation dehydration of isopropanol. Journal of Membrane Science 2006; 815-823.

[31] Kanti P, Srigowri K, Madhuri J, Smitha B, Sridhar S. Dehydration of ethanol through blend membranes of chitosan and sodium alginate by pervaporation. Separation and Purification Technology 2004; 40:259-266.

[32] Baker, RW. Membrane Technology and Applications. New York: McGraw-Hill, 2000. Ch.11.

[33] Hess S, Staudt-Bickel C, Lichtenthaler RN. Propene/propane separation with copolyimide membranes containing silver ions. Journal of Membrane Science 2006; 275:52-60.

[34] Kim JH, Min BR, Wong J, Kang YS. Complexation mechanism of olefin with silver ions dissolved in a polymer matrix and its effect on facilitated olefin transport. Chemistry – A European Journal 2002; 8(3):650-654.

[35] Ryu JH, Lee H, Kim YJ, Kang YS, Kim HS. Facilitated olefin transport by reversible olefin coordination to silver ions in a dry cellulose acetate membrane. Chemistry – A European Journal 2001; 7(7):1525-1529.

[36] Kang SW, Kim JH, Oh KS, Won J, Char K, Kim HS, Kang YS. Highly stabilized silver polymer electrolytes and their application to facilitated olefin transport membranes. Journal of Membrane Science 2004; 236:163-169.

[37] Liu L, Feng X, Chakma A. Unusual behavior of poly(ethylene oxide)/AgBF4 polymer electrolyte membranes for olefin-paraffin separation. Separation and Purification Technology 2004; 38:255-263.

[38] Yang JS, Hsiue GH. Selective olefin permeation through Ag(I) contained silicone rubber-graft-poly(acrylic acid) membranes. Journal of Membrane Science 1997; 139-149.

[39] Furr JR, Russell AD, Turner TD, Andrews A. Antibacterial activity of Actisorb Plus, Actisorb and silver nitrate. Journal of Hospital Infection 1994; 27:201-208.

[40] Parikh DV, Fink T, Rajasekharan K, Sachinvala ND, Sawhney APS, Calamari TA. Antimicrobial silver/sodium carboxymethyl cotton dressings for burn wounds. Textile Research Journal 2005; 75(2):134-138.

[41] Ueno H, Yamada H, Tanaka I, Kaba N, Matsuura M, Okumura M, Kadosawa T, Fujinaga T. Accelerating effects of chitosan for healing at early phase of experimental open wound in dogs. Biomaterials 1999; 20:1407-1414.

[42] Cho YW, Cho YN, Chung SH, Yoo G, Ko SW. Water-soluble chitin as a wound healing accelerator. Biomaterials 1999; 20:2139-2145.

[43] Du CH, Zhu BK, Chen JY, Xu YY. Metal ion permeation properties of silk fibroin/chitosan blen membranes. Polymer International 2006; 55:377-382

[44] Schussler A, Bellucci F, Senturia SD, and Latanision RM. Na^+ and Cl^- transport across polyimide films. Journal of Applied Polymer Science 1991; 42:1567-1577

[45] Henry F. Introduction to Chemical Engineering Analysis Using Mathematica. San Diego: Academic Press; 2002. Ch. 5.

[46] Tuwiner SB. Diffusion and Membrane Technology. New York: Reinhold Publishing; 1962.

[47] Daynes HA. The process of diffusion through a rubber membrane. Proceedings of the Royal Society of London 1920; 97(A):286-307.

[48] Barrer RM. Permeation, diffusion, and solution of gases. Transactions of the Faraday Society 1939; 35:628.

[49] Rutherford SW and Do DD. Review of time lag permeation technique as a method for characterization of porous media and membranes. Adsorption 1997; 3:283-312.

[50] Crank J, Park GS. Diffusion in Polymers. London: Academic Press; 1968.

[51] Jost W. Diffusion in Solids, Liquids, Gases. New York: Academic Press; 1960. Ch.1.

[52] Taveira P, Mendes A, Costa C. On the determination of diffusivity and sorption coefficients using different time lag models. Journal of Membrane Science 2003; 221:123-133.

[53] Favre E, Morliere N, Roizard D. Experimental evidence and implications of an imperfect upstream pressure step for the time-lag technique. Journal of Membrane Science 2002; 207:59-72.

[54] Haraya K, Obata K, Hakuta T, Yoshitome H. Permeation of gases through a symmetric cellulose acetate membrane. Journal of Chemical Engineering of Japan 1985; 464-466.

[55] Ye X, Lv L, Zhao XS, Wang K. Permeation time lag in polymeric hollow fiber membranes. Journal of Membrane Science 2006; 283:425-429.

[56] Galiatsatou P, Kanellopoulos NK, Petropoulos JH. Characterization of the transport properties of membrane of uncertain macrosopic structural homogeneity. Journal of Membrane Science 2006; 280:634-642.

[57] Kuhn DK, Johnson HH. Transient analysis of hydrogen permeation through nickel membranes. Acta Metallurgica et Materialia 1991; 39(11):2901-2908.

[58] Castellote M, Andrade C, Alonso C. Measurement of the steady and non-steady-state chloride diffusion coefficients in a migration test by means of monitoring the conductivity in the anolyte chamber Comparison with natural diffusion tests. Cement and Concrete Research 2001; 31:1411-1420.

[59] McCabe WL, Smith JC, Harriot P. Unit Operations of Chemical Engineering. Boston: McGraw Hill; 2001. Ch.26.

[60] Do DD. Adsorption Analysis: Equilibria and Kinetics. London: Imperial College Press; 1998.

[61] Zhao L. Removal of heavy metals from wastewater by adsorption using chitosan membranes. Waterloo: MASc Thesis, University of Waterloo; 2004.

[62] Ngah WW, Ghani SA, Kamari A. Adsorption behaviour of Fe(II) and Fe(III) ions in aqueous solution on chitosan and cross-linked chitosan beads. Bioresource Technology 2005; 96:443-450.

[63] Sag Y, Aktay Y. A comparative study for the sorption of Cu(II) ions by chitin and chitosan: application of equilibrium and mass transfer models. Separation Science and Technology 2002; 37(12):2801-2822.

[64] Ng JCY, Cheung WH, McKay G. Equilibrium studies for the sorption of lead from effluents using chitosan. Chemosphere 2003; 52:1021-1030.

[65] Nomanbhay SM, Palanisamy K. Removal of heavy metal from industrial wastewater using chitosan coated oil palm shell charcoal. Electronic Journal of Biotechnology 2005; 8(1):43-53.

[66] Neto AD, Neto EB, De Castro Dantas TN, De Paiva Telemaco E. Chromium adsorption by chitosan impregnated with microemulsion. Langmuir 2001; 17(14):4256-4260.

[67] Tan T, He X, Du W. Adsorption behaviour of metal ions on imprinted chitosan resin. Journal of Chemical Technology and Biotechnology 2001; 76:191-195.

[68] Al-ghezawi N, Şanli O, Işiklan N. Permeation and separation characteristics of acetic acid-water mixtures by pervaporation through acrylonitrile and hydroxyl ethyl methacrylate grafted poly(vinyl alcohol) membrane 2006; 41:2913-2931.

[69] Sag Y, Aktay Y. Kinetic studies on sorption of Cr(VI) and Cu(II) ions by chitin, chitosan and Rhizopus arrhizus. Biochemical Engineering Journal 2002; 12:143-153.

[70] Huang RYM, Yeom CK. Pervaporation separation of aqueous mixtures using crosslinked polyvinyl alcohol membranes. III. Permeation of acetic acid-water mixtures. Journal of Membrane Science 1991, 58:33-47.

Appendix A
Calibration Curves

The calibration curves used in this study are constructed by preparing $AgNO_3$ solutions of known concentration and measuring the conductivity. The conductivity values used for the concentration vs. conductivity plots have been deducted from that of the de-ionized water. The experimental data gathered for calibration are summarized in Table A.1, followed by the concentration vs. conductivity plot over the entire range of the data obtained (Fig. A.1). During the transient state of the permeation tests in this study, the conductivity of the receptor solution does not exceed 55 μS/cm. As a result, the curve used to convert the conductivity to concentration profile in the permeation tests only consists of calibration data up to a conductivity of 66μS/cm (Fig. A.2).

Table A.1 Calibration data

Concentration (M)	Conductivity (μS/cm)	De-ionized water (μS/cm)	Net conductivity (μS/cm)
3.00E-03	384	1.3	382.7
2.50E-03	325	0.9	324.1
2.00E-03	261	1	260
1.75E-03	231	1	230
1.50E-03	193.7	1.3	192.4
1.00E-03	129.9	0.9	129
5.00E-04	65.8	0.9	64.9
4.00E-04	53.2	1	52.2
2.50E-04	33.6	0.9	32.7
2.20E-04	37	1	36
2.00E-04	27.4	1	26.4
1.75E-04	29.5	1	28.5
1.50E-04	25.3	0.9	24.4
1.25E-04	27.4	1	26.4
1.00E-04	17.8	1	16.8
s8.80E-05	15.4	1	14.4
6.00E-05	10.8	0.9	9.9
3.00E-05	6	0.9	5.1
1.50E-05	3.6	0.9	2.7
5.00E-07	2.6	1	1.6

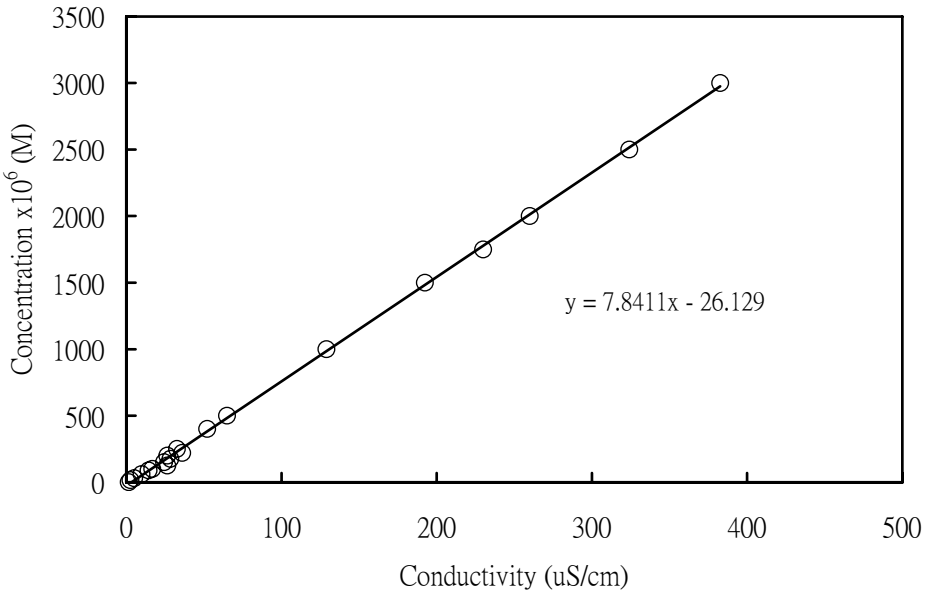

Figure A.1 Concentration vs. conductivity for conductivity up to 382.7 μS/cm.

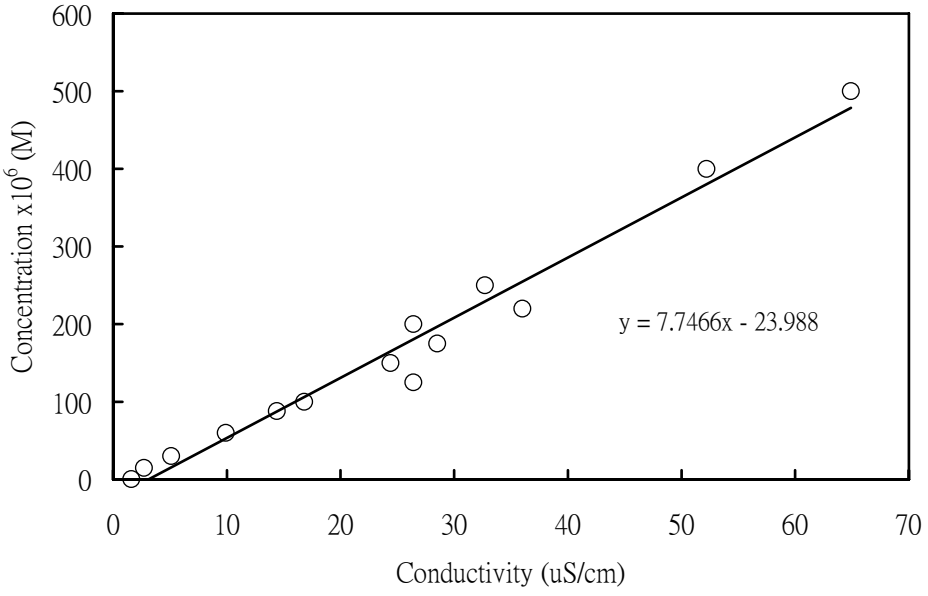

Figure A.2 Calibration curve used for permeation tests.

Appendix B
Experimental Data for Permeation Tests

The tables presented in Appendix B summarize the data for permeation tests at different conditions: Tables B.1-B.3 are related to the effect of feed $AgNO_3$ concentration, Tables B.4-B.6 the effect of membrane thickness, and Tables B.7-B.9 the effect of temperature. Data presented for each effect are corresponding to one another. That is, for example, data listed in the first row of Table B.1 are obtained from the same permeation test as the data listed in the first rows of Table B.2 and Table B.3.

Table B.1 Effect of feed $AgNO_3$ concentration on the diffusivity coefficient. (room temperature)

C_{1b} (M)	Time lag (s)	ℓ_o (μm)	R	Actual ℓ at transient permeation (μm)	D x 10^8 (cm^2/s)
0.69	26.32	25.4	1.48	37.5	8.92
0.48	26.08	24.8	1.48	36.6	8.58
0.11	227.35	26.2	1.48	38.7	1.10
0.26	76.75	26.5	1.48	39.2	3.33
0.40	45.63	24.7	1.48	36.5	4.87
0.48	40.96	26.7	1.48	39.5	6.33
0.56	34.63	24.9	1.48	36.8	6.52
0.64	26.96	26.4	1.48	39.0	9.41
0.78	27.73	26.9	1.48	39.8	9.50
0.83	28.12	26.6	1.48	39.3	9.16
1.00	23.27	26.3	1.48	38.9	10.82
0.73	32.31	25.4	1.48	37.5	7.27
0.98	28.55	24.9	1.48	36.8	7.91
0.90	25.58	25.3	1.48	37.4	9.11
0.08	262.81	25.0	1.48	36.9	0.87
0.18	104.08	25.1	1.48	37.1	2.20
0.36	50.05	25.6	1.48	37.8	4.77
0.11	188.07	18.7	1.48	27.6	0.68
0.22	115.24	17.2	1.48	25.4	0.93
1.02	19.98	19.1	1.48	28.2	6.65
0.58	33.37	16.6	1.48	24.5	3.01
0.87	20.53	16.8	1.48	24.8	5.00

(continued)

C_{1b} (M)	Time lag (s)	ℓ_o (μm)	*R*	Actual ℓ at transient permeation (μm)	D x 10^8 (cm^2/s)
0.18	64.12	18.6	1.48	27.5	1.96
0.36	27.33	18.7	1.48	27.6	4.66
0.64	18.93	19.2	1.48	28.4	7.09
0.80	21.81	19.3	1.48	28.5	6.22
0.77	29.64	18.9	1.48	27.9	4.39
0.26	36.84	17.3	1.48	25.6	2.96
0.55	24.94	17.5	1.48	25.9	4.47
0.83	24.57	19.4	1.48	28.7	5.58
0.98	23.61	19.3	1.48	28.5	5.74
0.11	188.07	18.7	1.48	27.6	0.68
0.50	21.49	19.7	1.48	29.1	6.57
1.02	19.98	19.1	1.48	28.2	6.65
0.30	36.04	20.0	1.48	29.6	4.04
0.79	24.22	21.3	1.48	31.5	6.82
0.18	64.12	18.6	1.48	27.5	1.96
0.36	27.33	18.7	1.48	27.6	4.66
0.64	18.93	19.2	1.48	28.4	7.09
0.80	21.81	19.3	1.48	28.5	6.22
0.77	29.64	18.9	1.48	27.9	4.39
0.83	24.57	19.4	1.48	28.7	5.58
0.98	23.61	19.3	1.48	28.5	5.74

Table B.2 Effect of feed $AgNO_3$ concentration on the permeation rate, permeance, and permeability coefficient (room temperature, receptor compartment 1.5L, membrane diameter 37mm)

C_{1b} (M)	$\Delta C_{2b}/\Delta t$ (mol/L s)	ℓ_o (μm)	*R*	Actual ℓ at SS[a] (μm)	J x 10^4 (mol/m^2 s)	P' x 10^4 [mol/m^2 s (mol/L)]	P x 10^8 [mol m/m^2 s (mol/L)]
0.69	1.55E-06	25.4	1.42	36.2	21.68	31.60	11.43
0.48	1.12E-06	24.8	1.44	35.7	15.67	32.73	11.70
0.11	8.13E-09	26.2	1.47	38.5	0.11	1.04	0.40
0.26	3.62E-07	26.5	1.46	38.6	5.05	19.74	7.63
0.40	6.67E-07	24.7	1.45	35.7	9.30	23.05	8.24
0.48	8.49E-07	26.7	1.44	38.5	11.84	24.89	9.58
0.56	1.02E-06	24.9	1.43	35.7	14.18	25.41	9.08
0.64	1.31E-06	26.4	1.43	37.7	18.25	28.29	10.66
0.78	1.63E-06	26.9	1.42	38.1	22.73	29.04	11.07
0.83	1.48E-06	26.6	1.41	37.6	20.69	24.91	9.36
1.00	1.89E-06	26.3	1.40	36.8	26.33	26.20	9.65

(continued)

C_{1b} (M)	$\Delta C_{2b}/\Delta t$ (mol/L s)	ℓ_o (μm)	R	Actual ℓ at SS[a] (μm)	J x 10^4 (mol/m^2 s)	P' x 10^4 [mol/m^2 s (mol/L)]	P x 10^8 [mol m/m^2 s (mol/L)]
0.73	1.43E-06	25.4	1.42	36.1	19.94	27.18	9.81
0.98	1.79E-06	24.9	1.40	34.9	24.96	25.46	8.89
0.90	1.77E-06	25.3	1.41	35.6	24.62	27.27	9.71
0.08	6.99E-08	25.0	1.47	36.8	0.98	12.95	4.76
0.18	2.24E-07	25.1	1.46	36.7	3.13	17.55	6.45
0.36	6.56E-07	25.6	1.45	37.1	9.15	25.31	9.39
0.11	9.40E-08	18.7	1.47	27.5	1.31	11.42	3.14
0.22	3.33E-07	17.2	1.46	25.1	4.64	21.47	5.39
1.02	2.43E-06	19.1	1.40	26.7	33.92	33.39	8.92
0.58	1.05E-06	16.6	1.43	23.8	14.63	25.37	6.03
0.87	2.03E-06	16.8	1.41	23.7	28.25	32.55	7.71
0.18	3.08E-07	18.6	1.46	27.2	4.29	24.08	6.56
0.36	8.07E-07	18.7	1.45	27.1	11.26	30.91	8.38
0.64	1.58E-06	19.2	1.43	27.4	21.98	34.51	9.46
0.80	1.74E-06	19.3	1.42	27.3	24.32	30.58	8.36
0.77	1.69E-06	18.9	1.42	26.8	23.54	30.70	8.23
0.26	5.79E-07	17.3	1.46	25.2	8.08	30.74	7.75
0.55	1.36E-06	17.5	1.44	25.1	18.94	34.33	8.62
0.83	1.89E-06	19.4	1.41	27.4	26.36	31.63	8.67
0.98	2.21E-06	19.3	1.40	27.1	30.88	31.47	8.52
0.11	9.40E-08	18.7	1.47	27.5	1.31	11.42	3.14
0.50	1.28E-06	19.7	1.44	28.3	17.91	35.70	10.12
1.02	2.43E-06	19.1	1.40	26.7	33.92	33.39	8.92
0.30	6.06E-07	20.0	1.45	29.1	8.46	28.65	8.34
0.79	1.82E-06	21.3	1.42	30.2	25.37	31.99	9.65
0.18	3.08E-07	18.6	1.46	27.2	4.29	24.08	6.56
0.36	8.07E-07	18.7	1.45	27.1	11.26	30.91	8.38
0.64	1.58E-06	19.2	1.43	27.4	21.98	34.51	9.46
0.80	1.74E-06	19.3	1.42	27.3	24.32	30.58	8.36
0.77	1.69E-06	18.9	1.42	26.8	23.54	30.70	8.23
0.83	1.89E-06	19.4	1.41	27.4	26.36	31.63	8.67
0.98	2.21E-06	19.3	1.40	27.1	30.88	31.47	8.52

[a] steady state of permeation

Table B.3 Diffisivity coefficients determined from the steady state permeation rate (D*) for different feed $AgNO_3$ concentrations (room temperature)

C_{1b} (M)	ΔC_m (mol/m^3)	Actual ℓ at steady state of permeation (μm)	$\Delta C_m/\ell$ (mol/m^4)	D* x 10^8 (cm^2/s)
0.69	1.44E+03	36.2	7.51E+07	28.85
0.48	1.36E+03	35.7	7.24E+07	21.64
0.11	1.03E+03	38.5	5.31E+07	0.21
0.26	1.22E+03	38.6	6.10E+07	8.27
0.40	1.32E+03	35.7	7.07E+07	13.17
0.48	1.36E+03	38.5	6.72E+07	17.62
0.56	1.40E+03	35.7	7.40E+07	19.16
0.64	1.43E+03	37.7	7.15E+07	25.51
0.78	1.47E+03	38.1	7.26E+07	31.32
0.83	1.48E+03	37.6	7.42E+07	27.90
1.00	1.53E+03	36.8	7.76E+07	33.92
0.73	1.46E+03	36.1	7.60E+07	26.24
0.98	1.52E+03	34.9	8.16E+07	30.59
0.90	1.50E+03	35.6	7.91E+07	31.11
0.08	9.51E+02	36.8	5.20E+07	1.88
0.18	1.14E+03	36.7	6.06E+07	5.16
0.36	1.30E+03	37.1	6.70E+07	13.67
0.11	1.05E+03	27.5	7.52E+07	1.74
0.22	1.19E+03	25.1	9.14E+07	5.08
1.02	1.53E+03	26.7	1.07E+08	31.67
0.58	1.40E+03	23.8	1.12E+08	13.11
0.87	1.49E+03	23.7	1.18E+08	23.87
0.18	1.14E+03	27.2	8.18E+07	5.25
0.36	1.30E+03	27.1	9.18E+07	12.27
0.64	1.43E+03	27.4	9.81E+07	22.40
0.80	1.48E+03	27.3	1.01E+08	23.97
0.77	1.47E+03	26.8	1.03E+08	22.88
0.26	1.23E+03	25.2	9.39E+07	8.60
0.55	1.39E+03	25.1	1.05E+08	18.02
0.83	1.49E+03	27.4	1.02E+08	25.90
0.98	1.52E+03	27.1	1.05E+08	29.32
0.11	1.05E+03	27.5	7.52E+07	1.74
0.50	1.37E+03	28.3	9.19E+07	19.50
1.02	1.53E+03	26.7	1.07E+08	31.67
0.30	1.25E+03	29.1	8.29E+07	10.21
0.79	1.47E+03	30.2	9.19E+07	27.62
0.18	1.14E+03	27.2	8.18E+07	5.25

(continued)

C_{1b} (M)	ΔC_m (mol/m^3)	Actual ℓ at steady state of permeation (μm)	$\Delta C_m/\ell$ (mol/m^4)	D* x 10^8 (cm^2/s)
0.36	1.30E+03	27.1	9.18E+07	12.27
0.64	1.43E+03	27.4	9.81E+07	22.40
0.80	1.48E+03	27.3	1.01E+08	23.97
0.77	1.47E+03	26.8	1.03E+08	22.88
0.83	1.49E+03	27.4	1.02E+08	25.90
0.98	1.52E+03	27.1	1.05E+08	29.32

Table B.4 Effect of membrane thickness on the diffusivity coefficient (Feed $AgNO_3$ concentration 1.0M, room temperature)

ℓ_o (μm)	Time lag (s)	*R*	Actual ℓ at transient permeation (μm)	D x 10^8 (cm^2/s)
22.0	18.13	1.48	32.5	9.72
24.7	21.01	1.48	36.5	10.59
19.7	20.66	1.48	29.2	6.86
23.7	21.04	1.48	35.1	9.74
22.7	20.65	1.48	33.6	9.10
28.3	30.96	1.48	41.8	9.40
23.2	22.96	1.48	34.3	8.52
33.6	32.10	1.48	49.7	12.83
28.0	27.13	1.48	41.4	10.52
42.0	36.23	1.48	62.1	17.72
36.9	33.05	1.48	54.5	15.00
47.3	40.50	1.48	69.9	20.08
27.5	21.71	1.48	40.7	12.72
49.3	49.07	1.48	72.8	18.01
45.6	41.39	1.48	67.4	18.31
50.2	48.21	1.48	74.2	19.01
22.2	18.33	1.48	32.8	9.77
27.0	23.73	1.48	39.9	11.18
36.4	35.39	1.48	53.7	13.60
24.1	25.23	1.48	35.6	8.37
21.6	21.83	1.48	31.9	7.78
24.2	25.15	1.48	35.8	8.48

Table B.5 Effect of membrane thickness on the permeation rate, permeance, and permeability (feed $AgNO_3$ concentration 1.0M, room temperature, receptor compartment 1.5L, membrane diameter 37mm)

ℓ_o (μm)	R	Actual ℓ at SS[a] (μm)	$\Delta C_{2b}/\Delta t$ (mol/L s)	J x 10^4 (mol/m^2 s)	P' x 10^4 [mol/m^2 s (mol/L)]	P x 10^8 [mol m/m^2 s (mol/L)]
22.0	1.40	30.8	2.48E-06	34.53	34.53	10.64
24.7	1.40	34.6	2.43E-06	33.96	33.96	11.76
19.7	1.40	27.6	2.42E-06	33.77	33.77	9.33
23.7	1.40	33.2	2.12E-06	29.58	29.58	9.83
22.7	1.40	31.8	1.79E-06	25.02	25.02	7.97
28.3	1.40	39.6	1.53E-06	21.34	21.34	8.45
23.2	1.40	32.5	2.10E-06	29.35	29.35	9.53
33.6	1.40	47.1	1.73E-06	24.19	24.19	11.40
28.0	1.40	39.2	1.76E-06	24.62	24.62	9.65
42.0	1.40	58.8	1.47E-06	20.51	20.51	12.07
36.9	1.40	51.7	1.71E-06	23.86	23.86	12.33
47.3	1.40	66.2	1.39E-06	19.44	19.44	12.87
27.5	1.40	38.6	2.31E-06	32.17	32.17	12.41
49.3	1.40	69.0	1.20E-06	16.79	16.79	11.59
45.6	1.40	63.9	1.31E-06	18.27	18.27	11.67
50.2	1.40	70.3	1.24E-06	17.29	17.29	12.15
22.2	1.40	31.1	3.05E-06	42.57	42.57	13.23
27.0	1.40	37.8	2.02E-06	28.20	28.20	10.67
36.4	1.40	50.9	1.49E-06	20.76	20.76	10.57
24.1	1.40	33.7	2.40E-06	33.49	33.49	11.30
21.6	1.40	30.3	2.18E-06	30.36	30.36	9.18
24.2	1.40	33.9	1.95E-06	27.27	27.27	9.24

[a] steady state of permeation

Table B.6 Diffisivity coefficients determined from the steady state permeation rate (D*) for different membrane thicknesses (feed $AgNO_3$ concentration 1.0M, room temperature)

ℓ_o (μm)	C_{1b} (M)	ΔC_m (mol/m^3)	Actual ℓ at steady state of permeation (μm)	$\Delta C_m/\ell$ (mol/m^4)	D* x 10^8 (cm^2/s)
22.0	1.0	1.53E+03	30.8	9.27E+07	37.24
24.7	1.0	1.53E+03	34.6	8.25E+07	41.18
19.7	1.0	1.53E+03	27.6	1.03E+08	32.66
23.7	1.0	1.53E+03	33.2	8.60E+07	34.41
22.7	1.0	1.53E+03	31.8	8.97E+07	27.89
28.3	1.0	1.53E+03	39.6	7.21E+07	29.58

ℓ_o (μm)	C_{1b} (M)	ΔC_m (mol/m^3)	Actual ℓ at steady state of permeation (μm)	$\Delta C_m/\ell$ (mol/m^4)	D* x 10^8 (cm^2/s)
23.2	1.0	1.53E+03	32.5	8.80E+07	33.36
33.6	1.0	1.53E+03	47.1	6.06E+07	39.90
28.0	1.0	1.53E+03	39.2	7.28E+07	33.80
42.0	1.0	1.53E+03	58.8	4.86E+07	42.24
36.9	1.0	1.53E+03	51.7	5.53E+07	43.18
47.3	1.0	1.53E+03	66.2	4.31E+07	45.07
27.5	1.0	1.53E+03	38.6	7.40E+07	43.45
49.3	1.0	1.53E+03	69.0	4.14E+07	40.56
45.6	1.0	1.53E+03	63.9	4.47E+07	40.87
50.2	1.0	1.53E+03	70.3	4.06E+07	42.55
22.2	1.0	1.53E+03	31.1	9.19E+07	46.30
27.0	1.0	1.53E+03	37.8	7.55E+07	37.34
36.4	1.0	1.53E+03	50.9	5.61E+07	37.02
24.1	1.0	1.53E+03	33.7	8.47E+07	39.56
21.6	1.0	1.53E+03	30.3	9.44E+07	32.15
24.2	1.0	1.53E+03	33.9	8.43E+07	32.35

Table B.7 Effect of temperature on the diffusivity coefficient (Feed $AgNO_3$ concentration 1.0M, average membrane thickness 21μm)

T (^{o}C)	ℓ_o (μm)	Time lag (s)	*R*	Actual ℓ at transient permeation (μm)	D x 10^8 (cm^2/s)
21.1	21.6	24.61	1.48	31.92	6.90
30.1	21.1	25.28	1.48	31.18	6.41
35.1	22.4	23.32	1.48	33.10	7.83
46.7	20.2	17.21	1.48	29.85	8.63
51.3	21.1	15.93	1.48	31.18	10.17
56.5	19.5	14.14	1.48	28.82	9.79
60.9	20.1	16.36	1.48	29.70	8.99

Table B.8 Effect of temperature on the permeation rate, permeance, and permeability (feed $AgNO_3$ concentration 1.0M, average membrane thickness 21μm, receptor compartment 1.5L, membrane diameter 37mm)

T (^oC)	ℓ_o (μm)	R	Actual ℓ at SS[a] (μm)	$\Delta C_{2b}/\Delta t$ (mol/L s)	J x 10^4 (mol/m^2 s)	P' x 10^4 [mol/m^2 s (mol/L)]	P x 10^8 [mol m/m^2 s (mol/L)]
21.1	21.6	1.40	30.25	2.41E-06	33.57	33.57	10.16
30.1	21.1	1.40	29.55	2.62E-06	36.48	36.48	10.78
35.1	22.4	1.40	31.37	2.55E-06	35.64	35.64	11.18
46.7	20.2	1.40	28.29	3.34E-06	46.55	46.55	13.17
51.3	21.1	1.40	29.55	3.54E-06	49.33	49.33	14.58
56.5	19.5	1.40	27.31	5.16E-06	71.94	71.94	19.65
60.9	20.1	1.40	28.15	4.53E-06	63.24	63.24	17.80

[a] steady state of permeation

Table B.9 Diffisivity coefficients determined from the steady state permeation rate (D*) for different temperature (feed $AgNO_3$ concentration 1.0M, membrane thickness 21μm)

T (^oC)	C_{1b} (M)	ΔC_m (mol/m^3)	Actual ℓ at steady state of permeation (μm)	$\Delta C_m/\ell$ (mol/m^4)	D* x 10^8 (cm^2/s)
21.1	1.0	1.53E+03	30.25	9.44E+07	35.56
30.1	1.0	1.53E+03	29.55	9.67E+07	37.74
35.1	1.0	1.53E+03	31.37	9.11E+07	39.15
46.7	1.0	1.53E+03	28.29	1.01E+08	46.10
51.3	1.0	1.53E+03	29.55	9.67E+07	51.04
56.5	1.0	1.53E+03	27.31	1.05E+08	68.78
60.9	1.0	1.53E+03	28.15	1.01E+08	62.33

Appendix C
Experimental Data for Sorption Tests

In the sorption tests, the $AgNO_3$ solution used has a volume of 40mL and the membrane samples have a cross-sectional area of 1.22×10^{-3} m^2. Tables C.1 and C.2 are corresponding to each other (i.e., data in the same row of the two tables are from the same sorption test.)

Table C.2 Effect of $AgNO_3$ concentration on sorption uptake of $AgNO_3$ and H_2O in chitosan membranes (room temperature)

C_0 (M)	C_0 (mg/L)	m_o (g)	m_w (g)	m_d (g)	H_2O uptake[a]	$AgNO_3$ uptake[b]	q_e (mg/g)	C_e (mg/L)	C_e/q_e
0.071	1.20E+04	0.039	0.074	0.054	0.51	0.38	384.62	1.16E+04	30.20
0.176	2.99E+04	0.029	0.055	0.043	0.41	0.48	482.76	2.95E+04	61.14
0.258	4.38E+04	0.019	0.031	0.029	0.11	0.53	526.32	4.36E+04	82.82
0.359	6.10E+04	0.039	0.081	0.063	0.46	0.62	615.38	6.04E+04	98.22
0.470	7.99E+04	0.025	0.047	0.041	0.24	0.64	640.00	7.95E+04	124.16
0.563	9.57E+04	0.043	0.088	0.068	0.47	0.58	581.40	9.51E+04	163.56
0.633	1.08E+05	0.029	0.05	0.045	0.17	0.55	551.72	1.07E+05	194.20
0.803	1.36E+05	0.028	0.049	0.045	0.14	0.61	607.14	1.36E+05	224.03
0.847	1.44E+05	0.034	0.06	0.053	0.21	0.56	558.82	1.43E+05	256.54
0.998	1.70E+05	0.041	0.077	0.066	0.27	0.61	609.76	1.69E+05	276.96
0.009	1.48E+03	0.039	0.071	0.041	0.77	0.05	51.28	1.43E+03	27.91
0.005	8.01E+02	0.035	0.069	0.043	0.74	0.23	228.57	6.01E+02	2.63
0.001	2.10E+02	0.021	0.037	0.025	0.57	0.19	190.48	1.10E+02	0.58
0.044	7.41E+03	0.031	0.071	0.039	1.03	0.26	258.06	7.21E+03	27.92
0	0	0.045	0.111	0.045	1.47	0	0	0	-

[a] unit: (g H_2O/g chitosan)

[b] unit: (g $AgNO_3$/g chitosan)

Table C.3 Effect of $AgNO_s$ concentration on membrane thickness and corresponding Ag^+ uptake on mol per volume basis (room temperature)

C_0 (M)	ℓ_o (μm)	ℓ_w (μm)	R	wet vol. of chitosan (m^3)	$AgNO_3$ adsorbed (g)	Ag^+ uptake (mol/m^3)
0.071	27.9	40.0	1.43	4.88E-08	0.015	1.81E+03
0.176	21.7	35.2	1.62	4.29E-08	0.014	1.92E+03
0.258	15.3	25.1	1.64	3.06E-08	0.010	1.92E+03
0.359	32.7	45.4	1.39	5.54E-08	0.024	2.55E+03
0.470	23.5	27.9	1.19	3.40E-08	0.016	2.77E+03
0.563	34.6	49.1	1.42	5.99E-08	0.025	2.46E+03
0.633	22.2	26.2	1.18	3.19E-08	0.016	2.95E+03
0.803	17.9	26.9	1.50	3.28E-08	0.017	3.05E+03
0.847	21.7	32.7	1.51	3.99E-08	0.019	2.81E+03
0.998	32.0	37.9	1.18	4.62E-08	0.025	3.18E+03
0.009	22.4	33.2	1.48	4.05E-08	0.002	2.91E+02
0.005	24.0	30.2	1.26	3.68E-08	0.008	1.28E+03
0.001	14.0	17.5	1.25	2.13E-08	0.004	1.10E+03
0.044	22.2	31.6	1.42	3.85E-08	0.008	1.22E+03
0	31.0	56.8	1.83	6.92E-08	0	0.00E+00

Table C.4 Effect of membrane thickness on sorption uptakse of $AgNO_3$ and H_2O in chitosan membranes and corresponding Ag^+ uptake on mol per volume basis ($AgNO_3$ concentration 1.0M, room temperature)

ℓ_o (μm)	m_o (g)	m_w (g)	m_d (g)	H_2O uptake[a]	$AgNO_3$ Adsorbed (g)	$AgNO_3$ uptake[b]	wet vol. chitosan (m^3)	Ag^+ uptake (mol/m^3)
33.0	0.035	0.077	0.06	0.49	0.025	0.71	4.68E-08	3.14E+03
19.3	0.027	0.054	0.045	0.33	0.018	0.67	3.11E-08	3.41E+03
48.8	0.079	0.166	0.132	0.43	0.053	0.67	8.68E-08	3.59E+03
24.4	0.033	0.069	0.055	0.42	0.022	0.67	3.52E-08	3.68E+03
35.8	0.044	0.087	0.073	0.32	0.029	0.66	5.27E-08	3.24E+03
31.9	0.046	0.103	0.077	0.57	0.031	0.67	5.75E-08	3.17E+03
23.4	0.032	0.068	0.052	0.50	0.020	0.63	4.13E-08	2.85E+03
28.0	0.037	0.077	0.059	0.49	0.022	0.59	4.35E-08	2.98E+03
19.5	0.027	0.058	0.045	0.48	0.018	0.67	3.30E-08	3.21E+03
15.5	0.019	0.037	0.031	0.32	0.012	0.63	2.77E-08	2.55E+03

[a] unit: (g H_2O/g chitosan)

[b] unit: (g $AgNO_3$/g chitosan)

Table C.5 Effect of membrane thickness on sorption uptake of $AgNO_3$ and H_2O in chitosan membranes and corresponding Ag^+ uptake on mol per volume basis ($AgNO_3$ concentration 0.5M, room temperature)

ℓ_o (μm)	m_o (g)	m_w (g)	m_d (g)	H_2O uptake[a]	$AgNO_3$ Adsorbed (g)	$AgNO_3$ uptake[b]	wet vol. chitosan (m^3)	Ag^+ uptake (mol/m^3)
36.2	0.051	0.106	0.078	0.55	0.027	0.53	6.45E-08	2.46E+03
34.9	0.058	0.12	0.088	0.55	0.030	0.52	7.07E-08	2.50E+03
50.8	0.053	0.114	0.082	0.60	0.029	0.55	7.51E-08	2.27E+03
23.6	0.032	0.066	0.048	0.56	0.016	0.50	3.78E-08	2.49E+03
21.8	0.029	0.061	0.044	0.59	0.015	0.52	3.63E-08	2.43E+03
16.5	0.021	0.047	0.034	0.62	0.013	0.62	3.10E-08	2.47E+03
33.1	0.045	0.096	0.068	0.62	0.023	0.51	5.64E-08	2.40E+03
35.4	0.053	0.111	0.078	0.62	0.025	0.47	6.39E-08	2.30E+03
24.4	0.032	0.065	0.048	0.53	0.016	0.50	4.38E-08	2.15E+03
19.7	0.026	0.053	0.039	0.54	0.013	0.50	3.35E-08	2.28E+03
16.0	0.024	0.048	0.037	0.46	0.01	0.54	2.85E-08	2.68E+03

[a] unit: (g H_2O/g chitosan)

[b] unit: (g $AgNO_3$/g chitosan)

TableC.6 Effect of temperature on sorption uptake of $AgNO_3$ and H_2O in chitosan membranes and corresponding Ag^+ uptake on mol per volume basis (feed $AgNO_3$ concentration 1.0M)

T (^oC)	m_o (g)	m_w (g)	m_d (g)	H_2O uptake[a]	$AgNO_3$ Adsorbed (g)	$AgNO_3$ uptake[b]	wet vol. chitosan (m^3)	Ag^+ uptake (mol/m^3)
30	0.018	0.035	0.028	0.39	0.010	0.56	2.29E-08	2.57E+03
40	0.032	0.068	0.051	0.53	0.019	0.59	3.90E-08	2.87E+03
50	0.031	0.061	0.048	0.42	0.017	0.55	3.67E-08	2.73E+03
63	0.031	0.072	0.051	0.68	0.020	0.65	4.07E-08	2.89E+03

[a] unit: (g H_2O/g chitosan)

[b] unit: (g $AgNO_3$/g chitosan)

Table C.7 Effect of temperature on membrane thickness

T (^oC)	ℓ_o (μm)	ℓ_w (μm)	R
30	14.3	18.8	1.31
40	22	32	1.45
50	22.6	30.1	1.33
63	22.6	33.4	1.48

Appendix D
Sample Calculations

Determination of the permeation parameters

Values used in this sample calculation are corresponding to the first rows of Table B.1 –B.3:

Original membrane thickness l_o = 25.4 μm

Diameter of membrane = 37mm

Cross sectional area of membrane A = 1.075×10^{-3} m^2

Volume of the receptor compartment V = 1.5L

Feed $AgNO_3$ concentration C_{1b} = 0.6861M

Time lag $\tau = 26.32s$

Slope of the $AgNO_3$ concentration in the receptor compartment vs. time

$$\frac{\Delta C_{2b}}{\Delta t} = 1.5539 \times 10^{-6} \frac{mol}{Ls}$$

Diffusivity $D = \frac{l^2}{6\tau}$

Linear regression for the relationship presented by Fig. 4.12 yields $y = -0.1546x + 1.4778$, where y = R, wet membrane thickness at sorption equilibrium / original membrane thickness before sorption, and x = $AgNO_3$ concentration (M). At the transient state, the concentration of AgNO3 inside the membrane is approximately zero.

$R = -0.1546 \times 0 + 1.4778 = 1.4778$

membrane thickness at transient state: $l = l_o \times R = 25.4 \times 1.4778 = 37.5$ μm

$$D = \frac{l^2}{6\tau} = \frac{(37.6\mu m)^2}{6 \times 26.32s} = 8.92 \frac{cm^2}{s}$$

Permeation rate $J = \frac{\Delta C_{2b}}{\Delta t} \times \frac{V}{A}$

$$J = 1.5539\times10^{-6}\,\frac{mol}{Ls}\times\frac{1.5L}{1.075\times10^{=3}\,m^2} = 21.68\times10^{-4}\,\frac{mol}{m^2 s}$$

Permeance $P' = \dfrac{J}{C_{1b} - C_{2b}}$

$C_{2b} \cong 0$

$$P' = \frac{J}{C_{1b}} = \frac{21.68\times10^{-4}\,\dfrac{mol}{m^2 s}}{0.6861\dfrac{mol}{L}} = 31.60\times10^{-4}\,\frac{mol}{m^2 s(\dfrac{mol}{L})}$$

Permeability $P = P'\times l$

At the steady state, R is estimated as

$$\frac{1}{2}\left[(-0.1546\times0+1.4778)+(-0.1546\times C_{1b}+1.4778)\right]$$

$$=\frac{1}{2}\left[(-0.1546\times0+1.4778)+(-0.1546\times0.6861+1.4778)\right]=1.4248$$

membrane thickness at the steady state $l = l_o \times R = 25.4\times1.4248 = 36.19\mu m$

$$P = 31.60\times10^{-4}\,\frac{mol}{m^2 s(\dfrac{mol}{L})}\times36.19\times10^{-6}\,m = 1.143\times10^{-7}\,\frac{molm}{m^2 s(\dfrac{mol}{L})}$$

Diffusivity coefficient determined using the steady state permeation rate (D*)

$$D^* = \frac{J\times l}{C_{1m} - C_{2m}}$$

$C_{2m} \cong 0$

l = membrane thickness at the steady state = 36.19 μm

Linear regression for the relationship shown in Fig. 4.13 yields

$y = 365.2\ln(x) + 2856.4$, where y = Ag^+ uptake (mol/m^3) and x = $AgNO_3$ concentration (M).

$$C_{1m} = 365.2\ln(C_{1b}) + 2856.4 = 365.2\ln(0.6861) + 2856.4 = 2718.82\frac{mol}{m^3}$$

$$D^* = \frac{21.68\times10^{-4}\ \frac{mol}{m^2 s}\times 36.19\mu m}{2718.82\frac{mol}{m^3}} = 2.885\times10^{-7}\ \frac{cm^2}{s}$$

Determination of the sorption parameters

Values used in this sample calculation are corresponding to the first rows of Table C.1 and C.2:

Diameter of membrane = 39.4 mm

Cross sectional area of membrane A = 1.2192×10^{-3} m^2

Volume of the $AgNO_3$ solution V = 0.04L

$AgNO_3$ concentration C_o = 0.071M

Original weight of dry membrane before sorption m_o = 0.039g

Wet weight of membrane after sorption m_w = 0.074g

Dry weight of membrane after sorption m_d = 0.054g

Original membrane thickness l_o = 27.9 μm

Wet thickness of membrane after sorption l_w = 40.0 μm

Molecular weight of $AgNO_3$ (MW) = 169.85 g/mol

$$C_o = 0.071M = 0.071\frac{mol}{L}\times 169.85\frac{g}{mol} = 11989\frac{mg}{L}$$

H_2O uptake = $\frac{m_w - m_d}{m_o} = \frac{0.074 - 0.054}{0.039} = 0.5128\frac{gH_2O}{gChitosan}$

$AgNO_3$ uptake = $\frac{m_d - m_o}{m_o} = \frac{0.054 - 0.039}{0.039} = 0.38462 \frac{gAgNO_3}{gChitosan}$

Parameters for sorption isotherm:

q_e = amount of $AgNO_3$ adsorbed by chitosan at equilibrium

$$q_e = \frac{m_d - m_o}{m_o} \times 1000 = 384.62 \frac{mg}{g}$$

C_e = concentration of $AgNO_3$ in the liquid phase at equilibrium

$$C_e = C_0 - \frac{q_e m_o}{V} = 11989 \frac{mg}{L} - \frac{384.62 \frac{mg}{g} \times 0.039 g}{0.04 L} = 11614 \frac{mg}{L}$$

$$R = \frac{l_w}{l_o} = \frac{40.0 \mu m}{27.9 \mu m} = 1.43$$

Ag^+ uptake in mol per volume basis

wet volume of chitosan at sorption equilibrium (v_w)

$$= A \times l_w = 1.2192 \times 10^{-3} m^2 \times 40.0 \mu m = 4.88 \times 10^{-8} m^3$$

$AgNO_3$ (g) adsorbed = m_d-m_o = 0.054-0.039 = 0.015 g

$$Ag^+ \text{ uptake } (\frac{mol}{m^3}) = \frac{\frac{AgNO_3(g)}{MW}}{v_w} = \frac{\frac{0.015 g}{169.87 \frac{g}{mol}}}{488 \times 10^{-8} m^3} = 1811 \frac{molAgNO_3}{m^3 Chitosan}$$

Appendix E
Error Analysis

The following plots demonstrate the reproducibility of experimental results in this study.

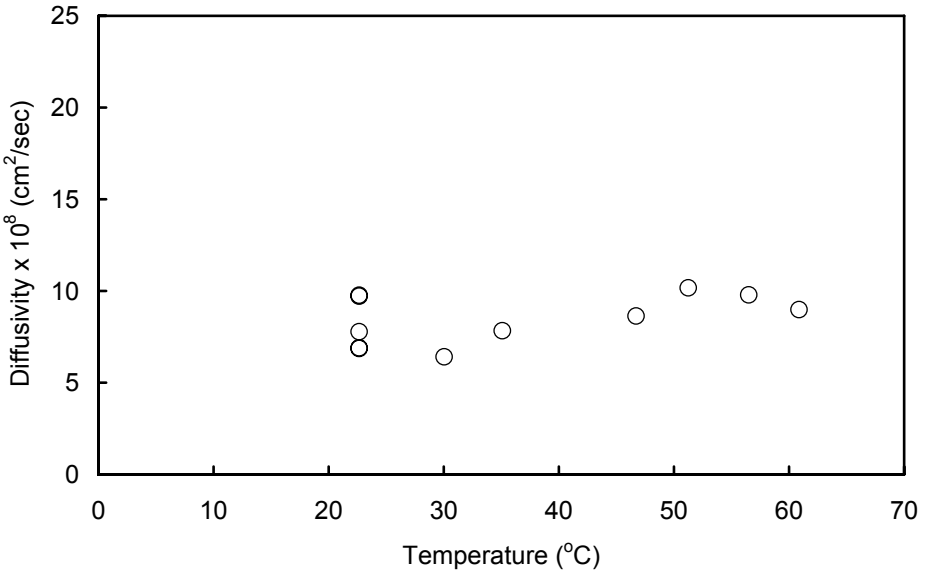

Figure E.1 Effect of temperature on diffusivity coefficient of Ag^+ through chitosan membranes. 5 data points are presented for diffusivity at room temperature (~23°C). Feed $AgNO_3$ concentration 1.0M, average membrane thickness 21μm.

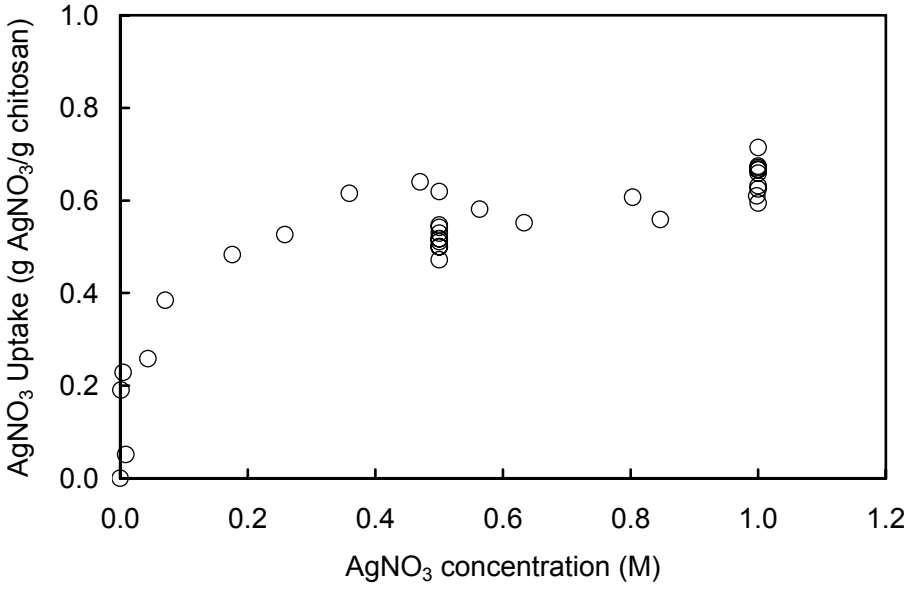

Figure E.2 Effect of $AgNO_3$ concentration on sorption uptake of $AgNO_3$ in chitosan membranes at room temperature. 10 data points are presented for $AgNO_3$ concentration of 1.0M and 11 for 0.5M.

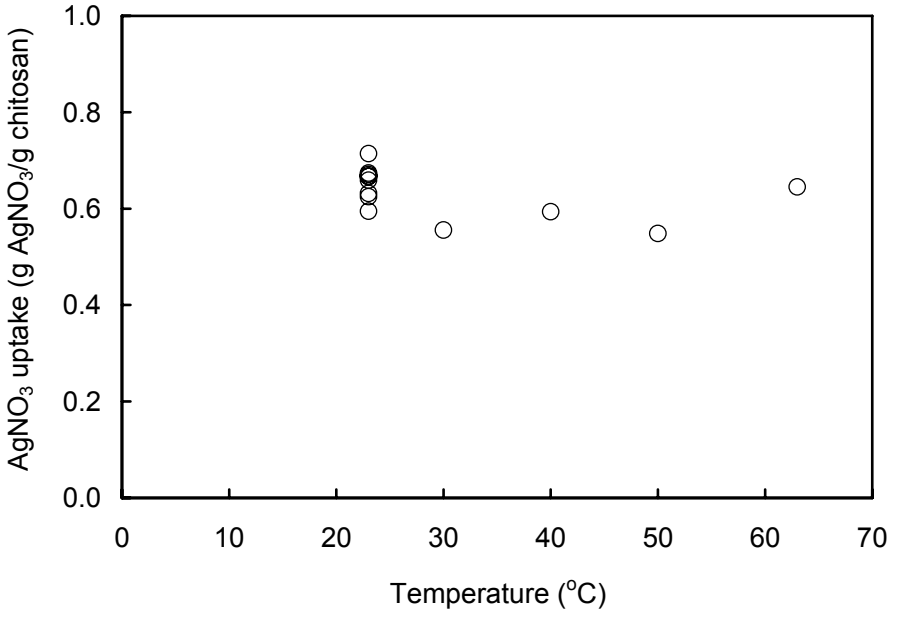

Figure E.3 Sorption uptake of $AgNO_3$ in chitosan membrane at different temperatures and at an $AgNO_3$ concentration of 1.0M. 9 data points are presented for room temperature (~23°C).